Volume 43 Number 7 July 1987

PHILIPS TECHNICAL REVIEW

Ion implantation

Laser-Doppler displacement meter

Schlieren method

PHILIPS

Philips Technical Review (ISSN 0031-7926) is published by Philips Research Laboratories, Eindhoven, the Netherlands, and deals with the investigations, processes and products of the laboratories and other establishments that form part of or cooperate with enterprises of the Philips group of companies. In the articles the associated technical problems are treated along with their physical or chemical background. The Review covers a wide range of subjects, each article being intended not only for the specialist in the subject but also for the non-specialist reader with a general technical or scientific training.

The Review appears in English and Dutch editions; both are identical in contents. There are twelve numbers per volume, each of about 32 pages. An index is included with each volume and indexes covering ten volumes are published (the latest one was included in Volume 40, 1982).

Editors:	Dr J. W. Broer
	Dipl.-Phys. R. Dockhorn, Editor-in-chief
	Dr E. Fischmann
	Dr J. L. Sommerdijk
	Ir N. A. M. Verhoeckx
	Dr M. H. Vincken
	Ir F. Zuurveen
Editorial assistants:	H. A. M. Lempens
	J. H. T. Verbaant
English edition:	D. A. E. Roberts, B.Sc., M. Inst. P., A.I.L.

© N.V. Philips' Gloeilampenfabrieken, Eindhoven, the Netherlands, 1987.
Articles may be reproduced in whole or in part provided that the source 'Philips Technical Review' is mentioned in full; photographs and drawings for this purpose are available on request. The editors would appreciate a complimentary copy.

PHILIPS TECHNICAL REVIEW

Volume 43, No. 7, July 1987

Contents

An open 800-kV ion-implantation machine 169
H. J. Ligthart and J. Politiek
The properties of silicon and metal surfaces can be radically altered by implanting high-energy ions

A laser-Doppler displacement meter 180
R. J. Asjes, C. S. Caspers and C. H. F. Velzel
Scattering from a moving pattern permits accurate measurement of velocity and displacement

Then and now (1937-1987) 183

Quantitative measurements by the Schlieren method 184
G. Prast
An optical method for the measurement of roughness and form of reflecting and transparent objects

Television test decor 192

Scientific publications 193

PHILIPS

PHILIPS

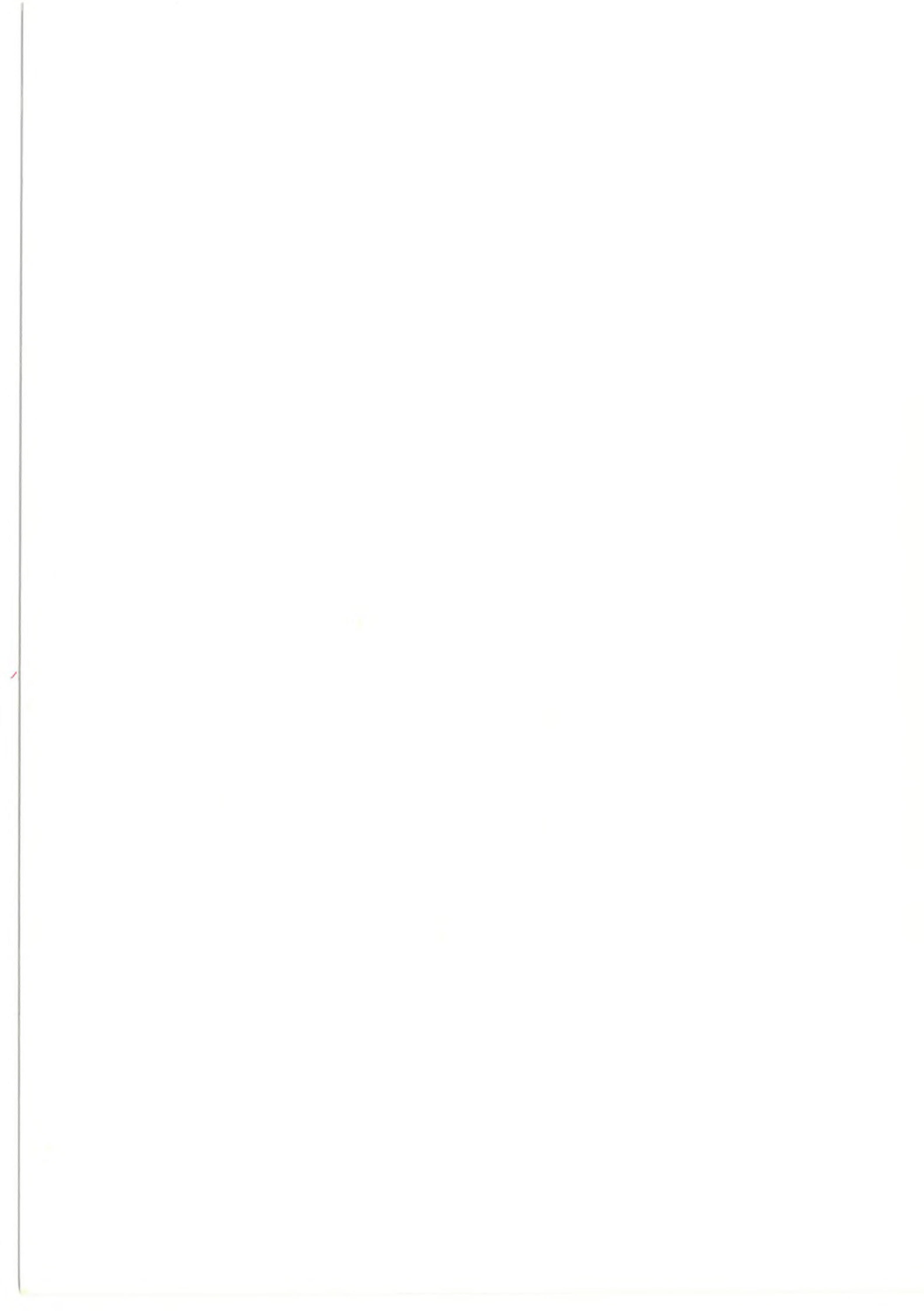

PHILIPS TECHNICAL REVIEW

Volume 43, No. 7, July 1987

An open 800-kV ion-implantation machine

H. J. Ligthart and J. Politiek

Conventional commercial ion-implantation machines are capable of implanting the usual donor and acceptor elements phosphorus, arsenic and boron in silicon. The accelerating voltage of these machines is generally no higher than 200 kV. If heavier elements are to be implanted in heavier substrates, higher accelerating voltages are required. In scientific research the ion source should also be easily interchangeable. In ion-implantation machines for accelerating voltages up to 1 MV, which are not normally commercially available, the high-voltage section is insulated from the environment by gas under pressure in a tank. Changing an ion source therefore takes a long time. The ion-implantation machine that has been developed at Philips Research Laboratories, however, has an 'open' high-voltage section, which is insulated from the environment by atmospheric air, so that the ion source can be changed very quickly.

Introduction

The object of ion implantation is to replace some of the atoms in a crystalline substance by other atoms that also fit into the lattice structure. The atoms of the element to be implanted are therefore ionized, accelerated to a high velocity in an electrostatic field and then implanted in the substrate. The resulting damage to the lattice can be removed by means of a heat treatment (annealing). Ion implantation is widely used in the manufacture of integrated circuits, for doping silicon with donors (e.g. phosphorus) or with acceptors (e.g. boron). An advantage of ion implantation as compared with thermal diffusion is that it is easier to control the concentration profile, i.e. the concentration (usually in cm^{-3}) as a function of depth. There is also much less lateral diffusion, and annealing times can be kept much shorter [1].

Fig. 1 shows a diagram of the concentration profile produced by a single implantation. (Other shapes of profile can be obtained by combining several implantations.) At a certain depth the concentration decreases sharply to zero, since the ions have completely lost their kinetic energy. Theoretically the dose (in cm^{-2}) is equal to the integral of the ion-flux density ϕ (in $cm^{-2}\,s^{-1}$) over time at the substrate surface. The dose is also equal to the integral of the concentration over the depth after the implantation. In practice a narrow ion beam that describes a fine raster is used, instead of a wide beam that covers the entire surface of the sub-

Dr H. J. Ligthart and Dr Ir J. Politiek are with Philips Research Laboratories, Eindhoven.

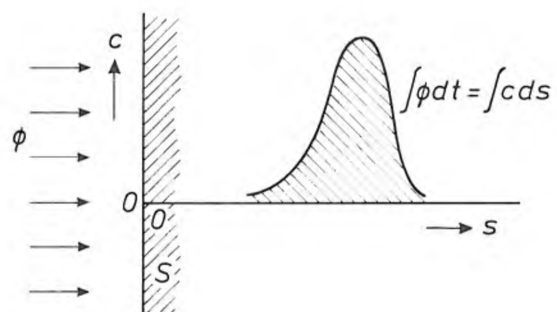

Fig. 1. Diagram of a concentration profile. *S* sample, typically a silicon slice, whose surface intersects the plane of the diagram at the vertical axis. *c* concentration of implanted ions. *s* depth from surface. ϕ ion-flux density. *t* time.

[1] W. K. Hofker and J. Politiek, Ion implantation in semiconductors, Philips Tech. Rev. **39**, 1-14, 1980;
S. T. Picraux and P. S. Peercy, Ion implantation of surfaces, Sci. Am. **252**, No. 3, 84-92, 1985.

strate. The spacing of the lines of the raster is less than the half-width of the beam cross-section. The mean ion-flux density is therefore equal to the beam current divided by the area of the raster. It follows that the height of the concentration profile is proportional to the beam current and to the duration of the implantation process. The location of the concentration profile depends on the kinetic energy of the ions and on the atomic numbers of the implanted element and the substrate material. If one of these two atomic numbers is increased, the profile moves towards the surface of the substrate. If the energy of the ions is increased, the profile moves into the material.

In the investigation of new materials for integrated circuits, use is made of heavier substrate materials (for example gallium phosphide, gallium arsenide or indium phosphide, known as III-V compounds) and heavier donors and acceptors (e.g. tellurium and cadmium). In research on integrated circuits it is also necessary to make deeper implantations, for example of oxygen ions to produce 'buried' SiO_2 layers. This accounts for the recent trend of implanting ions at higher kinetic energy.

Fig. 2 gives an idea of the collision processes that take place when ions move through a substrate. The diagram shows the ion-energy loss per unit pathlength as a function of the square root of the ion energy; the diagram is based on the LSS model (Lindhard, Scharff and Schiøtt) [2]. The straight line corresponds to the ion-energy loss resulting from collisions with electrons. These inelastic collisions cause no damage in the substrate. The curve corresponds to the energy loss due to collisions with nuclei. These elastic collisions do cause damage in the substrate. At a kinetic

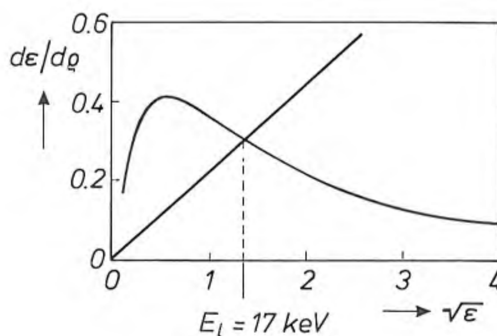

Fig. 2. The calculated energy loss per unit pathlength of the ions moving in the substrate as a result of collisions with nuclei of substrate atoms (curve) and with electrons (straight line), as a function of the square root of the energy of the ions as given by the LSS model [2]. To obtain a result valid for all elements, the 'reduced' quantities ϱ and ε are used for the path and the energy, respectively. If the ions have a higher kinetic energy than the threshold value E_l, the collisions with electrons predominate over those with nuclei. The slope of the straight line for the collisions with electrons is also a function of the atomic numbers of the ion and the substrate atoms. The diagram applies to the implantation of boron in silicon.

energy greater than E_l, at the intersection of the straight line and the curve, the inelastic collisions, which cause no damage, therefore predominate. (In implantations in silicon E_l is 17 keV for B^+ ions, 140 keV for P^+ ions, 800 keV for As^+ ions and 2000 keV for Sb^+ ions.) This means that with very deep implantations, with ions of high energy, relatively little lattice damage is caused at the substrate surface. Semiconductor structures already produced in the substrate should not therefore be damaged by implantations at greater depth.

How do we obtain ions of high kinetic energy? In the first place, of course, by increasing the strength of the electrostatic field, i.e. by increasing the potential at the ion source. (The substrate is normally at earth potential.) A higher energy can also be obtained by using multiply charged ions. A third method is to use a 'tandem' accelerator.

In a tandem accelerator the ion source is at earth potential. Single negatively charged ions from the source are accelerated and turned into positively charged ions (possibly multiply charged) in a 'stripper', consisting of a gas in a cell at positive potential. In this charge reversal one or more electrons are stripped from the ions by collisions with gas atoms. The positively charged ions then move towards the substrate, which is at earth potential. Disadvantages of tandem accelerators are that they have a low ion yield and are more complicated than single-ended accelerators.

The yield of an ion source generally decreases as the charge of the individual ions increases. Since the use of multiply charged ions instead of singly charged ions therefore results in a lower ion-flux density, the implantation time must be longer to produce a certain maximum concentration; see fig. 1. If deeper and more highly doped layers are required, implantation of multiply charged ions may not always be the right answer. Very deep implantations therefore require a high accelerating voltage, especially when heavy ions have to be implanted in heavy substrate material.

At Philips Research Laboratories in Eindhoven an ion-implantation machine has been developed, intended not only for research on new IC technologies but also for other work such as improving the hardness, wear resistance or corrosion resistance of metal surfaces. The high accelerating voltage of the machine, 800 kV, can be made even higher in the future. The machine was designed with an 'open' configuration, which means that the high-voltage section is not insulated by a gas (e.g. sulphur hexafluoride) under pressure in a tank, but is surrounded by atmospheric air at about 20 °C and at a relative humidity of less than 40 %. This makes it possible to change ion sources quickly. Some of the investigations on the machine are connected with the selection of ion

sources, since the effectiveness of the ion source largely determines the time required for an implantation. *Fig. 3a* shows the high-voltage section of the implantation machine with the acceleration tube on the right (the lower of the two tubes projecting through the wall). Fig. 3*b* shows the low-voltage section; the ions travel through this after they have passed through the acceleration tube.

In the following we shall first describe the construction of the implantation machine, and then we shall consider a few ion sources. The article concludes with a few examples of implantations to illustrate the usefulness of the machine.

a *b*

Fig. 3. Photograph of *a*) the high-voltage section and *b*) the low-voltage section of the 800-kV ion-implantation machine.

Construction of the implantation machine

Fig. 4 is a diagram of the machine. The high-voltage section contains the high-voltage generator *G*, the supply unit *SU* and the ion-source unit *IU*; see also fig. 3*a*. The low-voltage section contains the switching magnet *SM*, which directs the ion beam into one of the beam lines behind it. These beam lines terminate in the target chambers *TC1* and *TC2*, see also fig. 3*b*. The high-voltage section is surrounded by concrete walls 30 cm thick. The walls provide a shield against X-radiation due to the collision of electrons moving in the opposite direction to the beam. The walls of the high-voltage section are clad with metal foil to screen the environment from interfering electromagnetic fields.

The high-voltage generator *G* was designed by High Voltage Engineering of Amersfoort for a voltage of 1 MV. It is a conventional cascade generator of the Cockcroft and Walton type [3]. The generator is insulated from the environment by SF_6 gas at a slight excess pressure. The cascade circuit is supplied by an alternating voltage at 24 kHz and a maximum amplitude of 20 kV. The maximum voltage across each diode is therefore 40 kV. The generator can deliver a current of 2 mA via a copper-wire connection between the corona sphere (the upper part of the generator) and the supply unit *SU*, giving a maximum power of 2 kW. The sum of the ion-beam current and the leakage currents cannot therefore exceed 2 mA.

The supply unit *SU* contains two dynamos, each supplying a power of 12 kW. The dynamos are driven via insulating shafts by motors at earth potential in the basement below the high-voltage section. The dynamos provide the electrical energy for the various circuits, equipment and vacuum pumps in the units *SU* and *IU*. The unit *SU* also contains rectifier circuits that supply direct current to the magnet coils, and the electronic circuits for controlling the 'ion-optical' elements in *IU*. The control circuits communicate with the control console in the low-voltage section via optical-fibre connections. *SU* therefore also contains optoelectrical and electrooptical converters.

The unit *IU* contains the ion source, which is at a positive potential of 30 kV with respect to its immediate environment. The ions therefore arrive with a

[2] N. Bohr, The penetration of atomic particles through matter, K. Dan. Vidensk. Selsk. Mat.-Fys. Medd. **18**, No. 8, 1984 (144 pages);
J. Lindhard, M. Scharff and H. E. Schiøtt, Range concepts and heavy ion ranges; notes on atomic collisions II, K. Dan. Vidensk. Selsk. Mat.-Fys. Medd. **33**, No. 14, 1963 (39 pages).

[3] S. Gradstein, A modern high-voltage equipment, Philips Tech. Rev. **1**, 6-10, 1936;
A. Kuntke, A generator for very high direct current voltage, Philips Tech. Rev. **2**, 161-164, 1937.

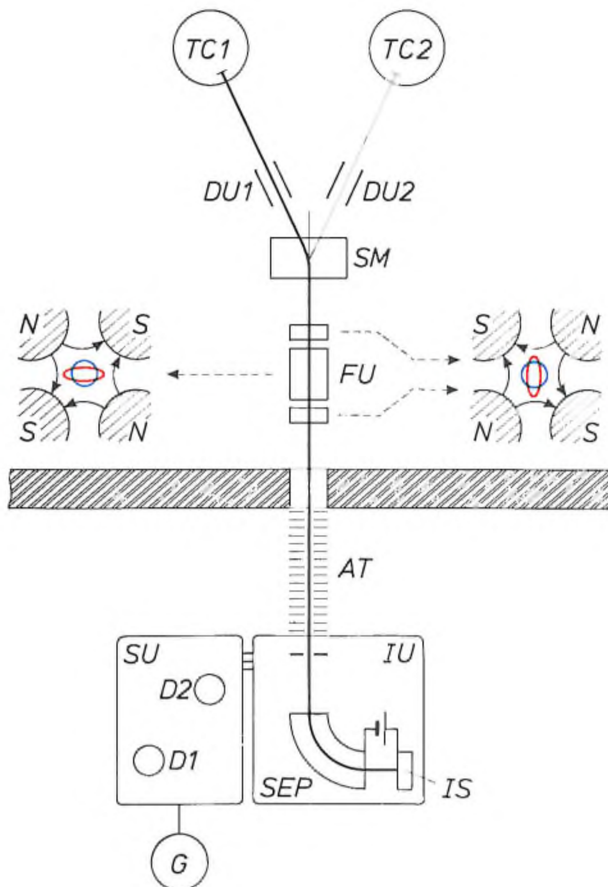

Fig. 4. Diagram of the ion-implantation machine. *G* high-voltage generator. *SU* supply unit. *D1*, *D2* dynamos. *IU* unit containing the ion source *IS*. *SEP* separator. The ion source is at a potential of 30 kV with respect to the separator. *AT* acceleration tube. *FU* focusing unit. This consists of three magnetic quadrupoles, whose action on the cross-section of the ion beam is illustrated in the separate diagrams on the left and right. *N*, *S* north and south poles of the quadrupoles. The beam cross-section in front of the quadrupole is shown in blue, the cross-section behind it is shown in red. *SM* switching magnet. *DU1* and *DU2* deflection units in the beam lines behind the switching magnet; see also fig. 6*d*. *TC1* and *TC2* target chambers.

certain initial velocity at the separator, which deflects them through an angle of 90° by means of a uniform magnetic field. The field-strength is adjusted so that the required ions pass through the exit slit while the unwanted ions do not. This follows from the expression for the radius R of the circular path of an ion in a magnetic field of flux density B [4]:

$$R = \frac{1}{B}\sqrt{\frac{2mE_{\mathrm{kin}}}{(ze)^2}}, \qquad (1)$$

where m is the mass of the ion, E_{kin} its kinetic energy, e the elementary charge and ze the charge of the ion. After the separator the ion beam enters the acceleration tube AT, which passes through the concrete wall between the high-voltage and low-voltage sections. The ions obtain the required kinetic energy in the acceleration tube. Turbomolecular pumps are connected to the ion source, the separator and the acceleration tube; these pumps keep the pressure low enough for the mean free path of the ions to be sufficiently large.

Putting the separator at high voltage has the advantage that the magnetic field does not need to be so powerful. If the separator were located after the acceleration tube, then as eq. (1) shows the magnetic flux density would have to be five to six times higher for the same radius. The units *SU* and *IU* are mounted on insulating columns. Parts of these columns connect metal plates, each at a defined potential; see fig. 3*a*. This is arranged by electrically interconnecting the plates by identical resistors, which have a total resistance of about 3.85 GΩ. Resistors are used in the same way to interconnect discs that distribute the potential drop linearly along the acceleration tube. These resistors are contained in another tube above the actual acceleration tube (see fig. 3*a*) and have a total resistance of 10 GΩ. The leakage currents through the resistors total 0.3 mA at 800 kV, so that the ion-beam current cannot exceed about 1.7 mA. In practice, however, the ion-beam current is always smaller.

In the low-voltage section the ion beam first passes through the focusing unit *FU*. This consists of a 'magnetic triplet', i.e. three magnetic quadrupoles in a row. Each of the quadrupoles corrects the beam cross-section in the vertical and horizontal directions. This can be seen from the shape of the lines of force in the quadrupoles as shown in fig. 4. The strength of each of the outer quadrupoles is half that of the inner quadrupole. The result is that the group of three quadrupoles has a converging action. As the ions leave the separator they diverge, and the divergence increases in the acceleration tube because they repel one another, but the divergence is almost completely compensated by the magnetic-triplet focusing unit. This therefore acts as a positive lens, which produces very nearly a point image of the beam cross-section at the exit of the separator on the sample in the target chamber. Astigmatism in the beam can be compensated by increasing the strength of one of the quadrupoles.

The ion beam next passes through the switching magnet *SM*, which works on the same principle as the separator in the high-voltage section. The direction of the field in the switching magnet is reversible, so that charged particles in the beam can be deflected clockwise or anticlockwise as desired, through an angle of ± 20°. The switching magnet also removes neutral particles from the beam. A third and important function of the switching magnet is the elimination of unwanted ions produced by charge exchange.

The effectiveness of the double separation of particles, in the separator and in the switching magnet, can be seen in the implantation of phosphorus, for ex-

ample. At moderate temperatures, phosphorus vapour consists of P_4 molecules. However, at a temperature of 800 °C, which is almost always exceeded in the ion source, the dissociation

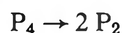

$$P_4 \rightarrow 2\,P_2$$

commences. The source thus contains P^+, P^{++} and P_2^+ ions. The P_2^+ ions may dissociate later in the reaction

$$P_2^+ \rightarrow P^+ + P.$$

If this happens at the inlet of the separator, the P^+ ions have a kinetic energy here of a quarter of that of the P^{++} ions. (We assume that the energy of a P_2^+ ion is evenly divided between the P^+ ion and the P atom.) It can be seen from eq. (1) that in this case the P^+ ions and the P^{++} ions describe a path of the same radius in the separator and are therefore not separated. It is easy to verify that these ions do in fact become separated in the switching magnet. (If an electrostatic deflection unit were to be used instead of a switching magnet, the P^+ and P^{++} ions would describe virtually the same parabolic path, so that these ions would not be separated.)

In each of the two beam lines following the switching magnet the ion beam can be moved horizontally and vertically by means of electrostatic deflection plates. At the entrance of each beam line there is a set of four short deflection plates, followed by a set of four long deflection plates, as shown in fig. 6*d*. The set of short plates is intended for deflecting ion beams of low energy, the set of long plates is for beams of high energy. The target chamber *TC1* is used for investigating various kinds of samples for other applications, unconnected with the manufacture of integrated circuits. Target chamber *TC2* is intended for implantations for IC manufacture. The slices are placed in a drum, which can accomodate 29 slices of diameter 100 mm. To comply with the clean-room conditions required in IC manufacture, target chamber *TC2* is placed in a special enclosure with a down-flow of filtered air. The vacuum is maintained by cryopumps to give a pressure of less than 10^{-7} mbar in the two beam lines and the target chambers [6].

Moving the beam over the sample

'Triangular' voltages applied to the horizontal and vertical deflection plates produce a uniform distribution of implanted ions over the specimen. The frequency of the triangular voltage for the horizontal deflection is 93 Hz; for the vertical deflection it is 800 Hz. Every 1/186 s the ion beam writes the pattern shown in blue in *fig. 5*. This pattern has

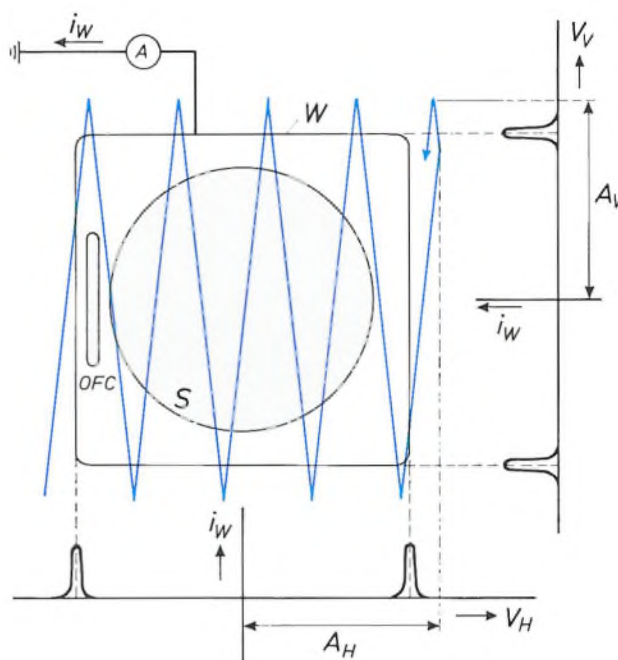

Fig. 5. The path (in blue) that the beam traces out on the sample during a half-period of the 'triangular' voltage for the horizontal deflection. *S* sample, typically a silicon slice. *OFC* opening of Faraday cup (*FC* in fig. 7). *W* wire frame, earthed via a milliammeter that measures the current i_W through the frame. The diagrams below and on the right correspond to the display on an oscilloscope screen when the vertical deflection in the oscilloscope is proportional to the current i_W and the horizontal deflection is proportional to the triangular voltage V_H or V_V on the horizontal or vertical deflection plates in the beam line. The diagram at the bottom of the figure is obtained with V_V set to 0; the diagram on the right is obtained with V_H set to 0. A_H and A_V are the amplitudes of V_H and V_V. The scales for V_H and V_V are chosen such that the distances between the peaks are equal to the width and height respectively of the wire frame.

$800/2 \times 93 \approx 4.3$ periods. In each second the beam writes 186 such patterns, all adjacent. After exactly one second the writing of 186 non-overlapping patterns is repeated.

During implantation it is necessary to ensure that the beam direction does not coincide with an 'open' crystal direction (a 'channel') of the sample, otherwise the penetration depth of the ions will vary considerably if the angle of incidence is not absolutely constant. Nor should the direction of the beam lie in a 'channel plane'. The sample is therefore rotated in its own plane through a predetermined angle and the beam meets the surface of the sample at an angle of 7° to the normal.

The usual requirement for the uniformity of an implantation is that the dose should not vary by more than 1 % over the sample. This means that the trian-

[4] J. F. Ziegler (ed.), Ion implantation, science and technology, Academic Press, Orlando, FL, 1984;
H. Ryssel and H. Glawischnig (ed.), Ion implantation techniques (Springer Ser. Electrophys., Vol. 10), Springer, Berlin 1982.

[6] J. J. Scheer and J. Visser, Application of cryopumps in industrial vacuum technology, Philips Tech. Rev. 39, 246-255, 1980.

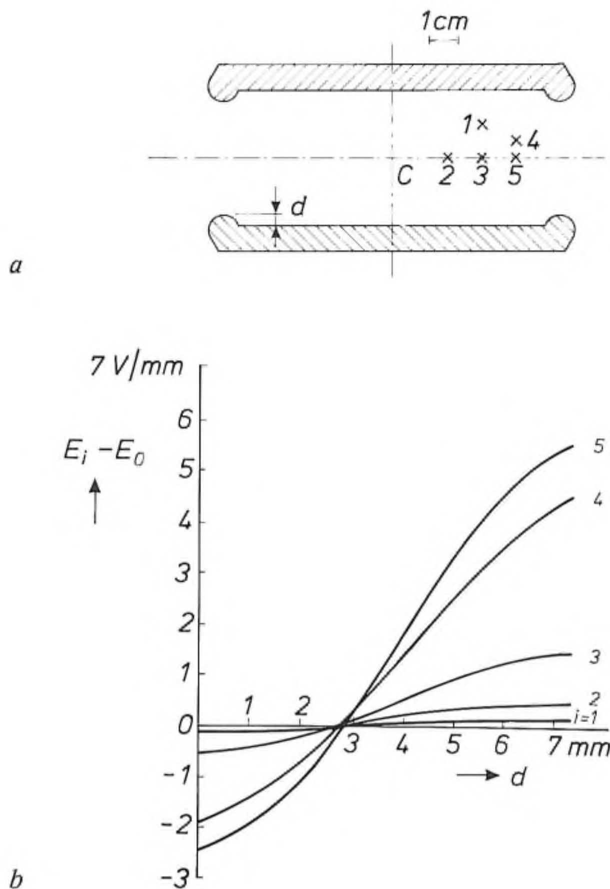

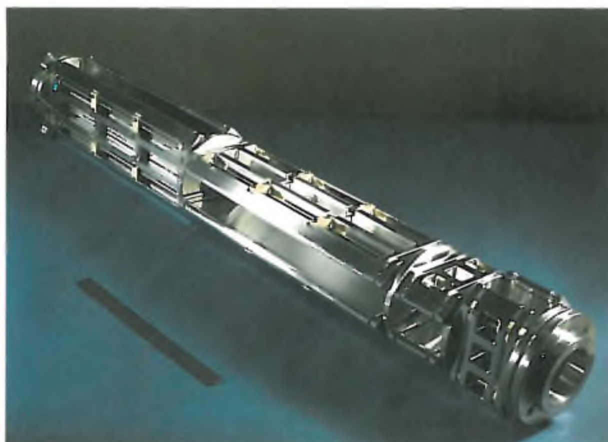

gular voltage should be highly linear. In addition, the field between the deflection plates should be homogeneous over the largest possible region. If flat deflection plates were used, the strength of the electric field would decrease towards the edges. The deflection of an ion would then depend on the position where the ion entered the region between the plates. (This position depends on the deflection produced by the preceding plates and on the dimensions of the beam cross-section.) With flat deflection plates the dose can vary by a high percentage. We have solved this problem by adding a 'lip' at the edges of the plates. We determined the height of the lip with the ELOP and GELOP software packages [6]. *Fig. 6* shows the shape of the deflection plates and the results of the computer calculations. For a lip 2.75 mm high the field is homogeneous over a very large region, and the dose produced by our implantation machine varies by no more than 0.5 % over the wafer.

The correct amplitudes A_H and A_V for the triangular voltages on the deflection plates are set up with the aid of a wire frame around the sample; see fig. 5. The wire frame is earthed through a milliammeter. While the amplitude of the voltage for the horizontal deflection is adjusted, the amplitude of the voltage for the vertical deflection is set to zero. If the vertical deflection on an oscilloscope is then made proportional to the current i_W through the wire frame and the horizontal deflection on the oscilloscope is made proportional to the voltage between the horizontal-deflection plates in the beam tube, the image that appears on the screen corresponds to the lower diagram in fig. 5. The location of the peaks on the oscilloscope screen shows how far the beam goes beyond the region inside the wire frame. The shape of the peak gives an idea of the half-width of the beam cross-section in the horizontal direction. A similar procedure is used for adjusting the voltage on the vertical deflection plates and estimating the half-width of the beam cross-section in the vertical direction.

The total number of ions incident on the sample — which is a measure of the average dose — is determined with the aid of a Faraday 'cup'. The opening in the Faraday cup is indicated by *OFC* in fig. 5. A diagram of the cross-section of the Faraday cup is shown

◁

Fig. 6. Calculation of the height *d* of the 'lip' on the deflection plates for the most uniform distribution of the electrostatic field. *a*) Cross-section of the deflection plates. At the points $i = 1$ to 5 the field-strength E_i was determined by the ELOP and GELOP software packages[6]. E_0 field-strength at the centre *C*: 120 V/mm. *b*) The difference $E_i - E_0$ between the field-strengths at the points *1* to *5* and at the centre as a function of *d*. For $d = 2.75$ mm the differences for these five points are virtually negligible. *c*) Photograph of a short deflection plate with lip. *d*) Photograph of the assembly of short and long deflection plates.

in *fig. 7*. The cup 'captures' all positively charged particles that pass through the opening. The sum of the charges of all these particles is measured by a current integrator. Electrode E_1 is at a low negative voltage, which ensures that secondary electrons generated on the outside wall of the cup do not enter the cup and affect the result of the measurement. Electrode E_2 captures the secondary electrons produced in the cup. Electrode E_3 captures positively charged particles of low energy, produced by ion collisions inside the cup. Electrode E_4 captures the ions from the beam that have passed through the opening of the cup. The currents through E_2 and E_3 also contribute to the measured result.

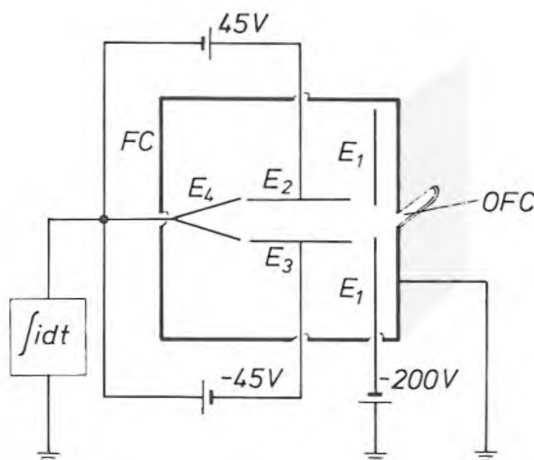

Fig. 7. Diagram of the cross-section of the Faraday cup *FC* with opening *OFC*; see fig. 5, and with the electrodes E_{1-4}. Electrode E_4 captures the ions from the beam. The result of the measurement with the current integrator connected to E_4 is a measure of the implantation dose. E_1 repels secondary electrons from outside the cup. The charged particles captured by E_2 and E_3 contribute to the measured result.

The ion sources

As we have seen, it is very important that the ion source in an ion-implantation machine should give a high current of the appropriate ions. We shall now discuss five ion sources that are used in our implantation machine. It will be shown that each source has its characteristic advantages and disadvantages. As noted earlier, the ion source in an implantation machine for research should be easy to change.

Ions are produced by collisions between electrons and atoms. To produce a singly charged ion the colliding electron should have an energy above a threshold value that is generally between 5 and 10 eV, depending on the element. (This threshold value expressed in volts is called the ionization potential.) To change a singly charged ion into a doubly charged ion the electron must have an energy higher than a threshold value of 15 to 30 eV. In general, doubly charged ions can be changed into triply charged ions at an electron energy higher than a threshold value of 30 to 100 eV. In the plasma generated in ion sources the electrons are therefore made to travel the greatest possible distance at a kinetic energy sufficiently high to produce the required ions. In four of the ion sources described here the electrons acquire their kinetic energy from an electrostatic field between an anode and a cathode. The fifth source makes use of microwaves for the energy transfer. The electrons are made to travel a long path through the action of a magnetic field, which forces the electrons into a helical path, whose radius is given by equation (1). The pressure in the source is a compromise. On the one hand a large number of ions is desirable, so there must be sufficient gas to supply these ions. On the other hand, it is undesirable for multiply charged ions to lose their charge through collisions with other particles. A pressure smaller than 10^{-2} mbar is normally used.

The ions produced are drawn from the source with the aid of an extraction electrode, located a short distance — about 5 mm — from the actual source and at a potential of − 30 kV with respect to the source. The extraction electrode is at the same time the input diaphragm for the separator; see fig. 4. Since the plasma is a good conductor, the boundary of the plasma corresponds to an equipotential surface, so that the ions leave the surface of the plasma perpendicularly. The gas pressure and the general discharge conditions in the source determine the shape of the plasma at the extraction aperture. Apart from the Maxwell-Boltzmann distribution, this shape and that of the extraction electrode thus determine the divergence of the ion beam as it leaves the source.

The five ion sources will now be briefly reviewed. (The sources in their original version were a product of High Voltage Engineering.)

The hollow-cathode source

Fig. 8 shows the principle of the hollow-cathode source, also known by the name of its first manufacturer as the Danfysik source. A great advantage of the source is that both gases and solids can be ionized. These are evaporated in a ceramic oven. The maximum oven temperature is 1500 °C, which is high enough for many elements to reach a sufficiently high vapour pressure. To produce ions of elements for which this does not apply, it is necessary to start from compounds. The difficulty with the use of compounds is that many unwanted ions are produced.

In the hollow-cathode source the electrons for the plasma are supplied by a filament which connects two

[6] K. J. van Oostrum, CAD in light optics and electron optics, Philips Tech. Rev. 42, 69-84, 1985.

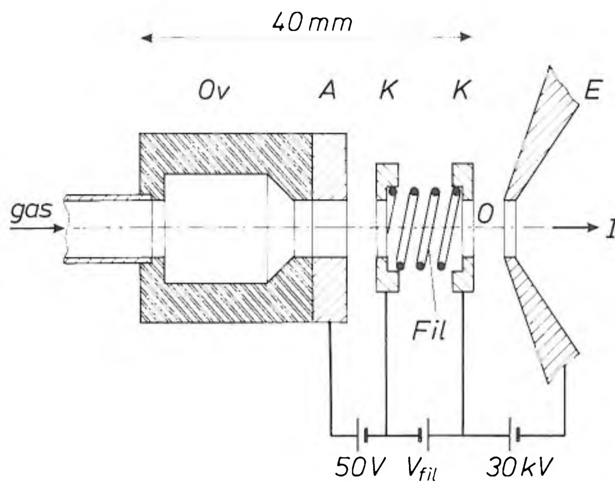

Fig. 8. The hollow-cathode source. *Ov* oven. *A* anode. *K* cathode, consisting of two parts. The two parts are connected by the filament *Fil*. V_{fil} filament voltage. *E* extraction electrode. *I* ion-beam current. The source contains a plasma that protrudes from the extraction aperture *O*.

parts of the cathode. A weak magnetic field is applied. A strong magnetic field is not necessary since the filament produces many electrons, giving rise to many ionizations. The anode-cathode voltage is low, about 50 V, to keep the anode-cathode current within bounds. Because of the low anode-cathode voltage the spread in the ion energy is small.

The versatility of the source makes it particularly suitable for research applications. There are a few disadvantages: the low anode-cathode voltage produces few doubly charged and multiply charged ions, the filament has a life of less than 24 hours, and the high temperatures of the filament and oven can cause unwanted reactions.

The Penning source

The Penning source, see *fig. 9*, does not have the disadvantages of the hollow-cathode source that result from the use of a filament. The operation of the Penning source, which is comparable with the well-known Penning gauge [7], is based on ionization with a high electric field-strength. The voltage between the anode and the cathodes is therefore high, 3 kV, and is more than enough to generate triply charged and multiply charged ions. A strong axial magnetic field makes the electrons move back and forth along helical paths between the two cathodes. The magnetic field is excited by a coil (not shown) mounted around the source.

The source is simple and reliable in use, requires little maintenance, and can produce a high current of multiply charged ions. It can generate, for example, a current of 0.1 μA of Ar^{4+} ions. (These ions therefore have a kinetic energy of 3 MeV at an accelerating voltage of 750 kV at the sample.) A disadvantage is that only gaseous elements and compounds can be ionized. Also, since the ions in the source move in a strong electrostatic field, their energy varies a great deal at the extraction aperture, so that the energy spread in the beam is considerable. If this energy spread is limited by using a narrow exit slit for the separator, the ion current is reduced. If a broad exit slit is used, unwanted ions pass through and the angular spread of the ion beam also increases.

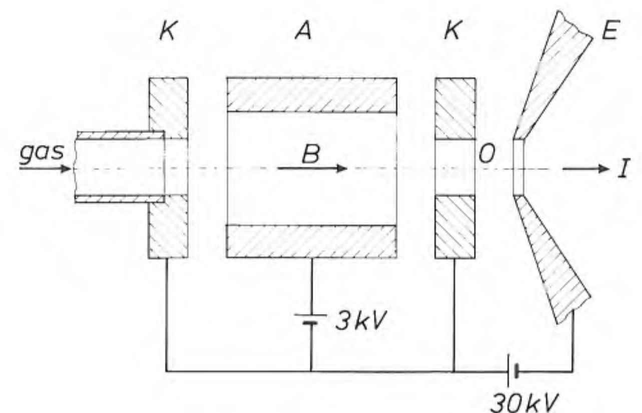

Fig. 9. The Penning source. The symbols have the same significance as in fig. 8. This source does not have a filament, but operates with a strong magnetic field of flux density *B*.

The radial Penning source

The radial-extraction Penning source, shown in *fig. 10*, does not have the disadvantage of a large spread in energy because the ions are extracted from one place in the plasma, where they all have about the same kinetic energy. Except for the ion extraction, this source is almost identical with the conventional Penning source. It has permanent magnets of samarium-cobalt for ease of construction.

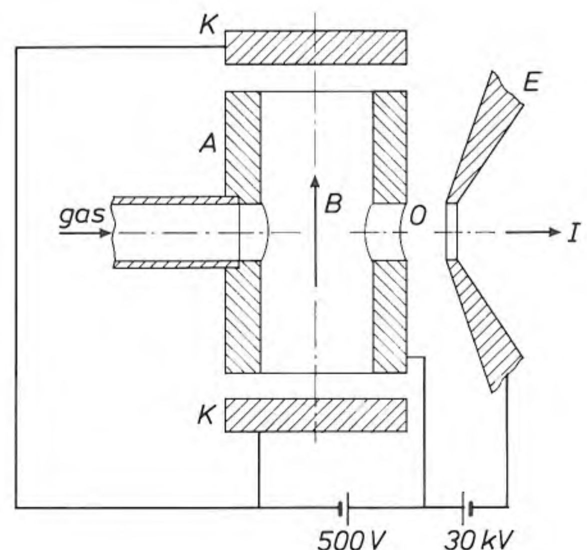

Fig. 10. The radial-extraction Penning source. The symbols have the same significance as in figs 8 and 9.

A disadvantage of this source is that it is necessary to use a high plasma density, which means that the anode-cathode current is high. The anode-cathode voltage associated with this current is about 500 V. The high current causes sputtering of cathode material, which means that the cathodes of the source have a shorter life than the cathodes of the conventional Penning source. This source is also only suitable for the ionization of gases, of course.

The sputter source

The sputter source, shown in *fig. 11*, has the special feature that it will ionize nearly all conducting solids whose melting point is not too low, including those with a very low vapour pressure (and usually a high melting point), e.g. tungsten and tantalum. This source also operates with a strong magnetic field; the anode-cathode voltage is about 180 V. The magnetic field is excited by a coil and can therefore be varied in magnitude.

The plasma is formed in argon gas. Ions of this gas collide with the cathode and sputter the cathode material. In the previous source this was a disadvantage, but here it is useful, because the two parts of the cathode are coated with the element to be ionized. The anode-cathode current must be high: 0.5 A. The ions formed at the part of the cathode near the extraction electrode contribute directly to the ion current. The ions formed at the other part of the cathode contribute much less since they cannot easily pass the anode. Indirectly, however, this part of the cathode does contribute to the ion current by generating neutral particles that are ionized later.

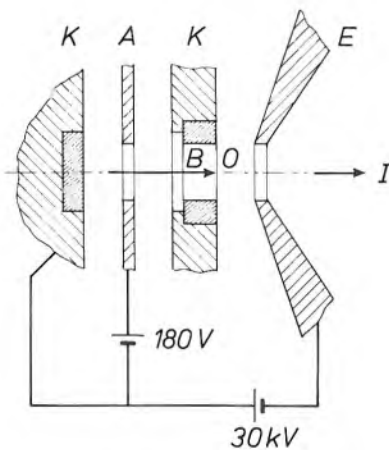

Fig. 11. The sputter source. The symbols have the same significance as in figs 8 and 9. The two parts of the cathode are coated with the element to be ionized.

With the sputter source we have obtained currents of 30 μA with Ta^{+} ions, 30 μA with Ta^{2+} ions, 6 μA with Ta^{3+} ions and 2 μA with Ta^{4+} ions. (A current of 1 μA corresponds to 6.25×10^{12} singly charged particles per second.) With other ion sources it is particularly difficult to ionize tantalum.

The microwave source

In the microwave source, shown in *fig. 12*, energy is not transferred to the plasma by an electrostatic field but by a microwave electromagnetic field generated by a magnetron [8].

The frequency of the microwave circuit, which is connected to the source by a coaxial line, is tuned to the cyclotron frequency of the electrons. An equation for this frequency can be found by substituting $E_{\text{kin}} = \frac{1}{2} m(2\pi fR)^2$ and $z = 1$ in equation (1):

$$f = \frac{Be}{2\pi m}. \tag{2}$$

The cyclotron frequency is thus the frequency of rotation of the electrons in their helical path in a constant magnetic field; this frequency is independent of the kinetic energy of the electrons. If the energy increases, the radius of the path becomes larger, but the frequency of rotation remains the same.

In our case the frequency of the travelling waves in the microwave circuit is approximately equal to

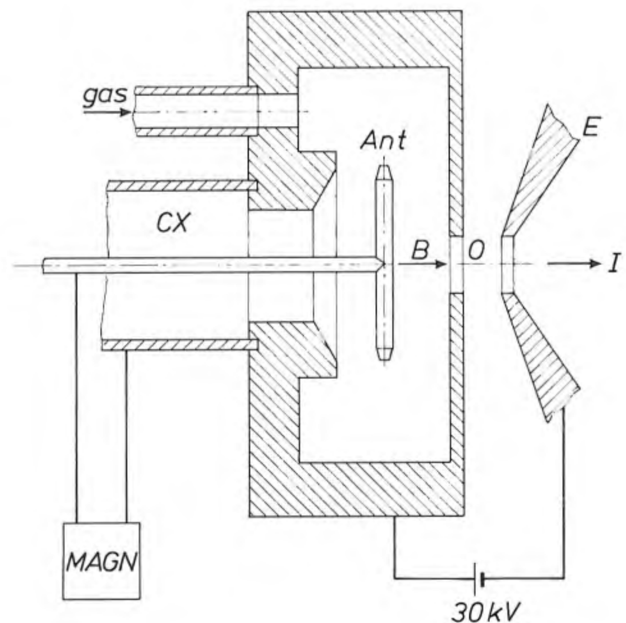

Fig. 12. The microwave source. This source is connected by a coaxial line *CX* to a magnetron *MAGN*, which supplies microwave energy to the plasma in the source. *Ant* antenna. See the captions to figs 8 and 9.

[7] F. M. Penning, High-vacuum gauges, Philips Tech. Rev. **2**, 201-208, 1937.
[8] J. Ishikawa, Y. Takeiri and T. Takagi, Axial magnetic field extraction-type microwave ion source with a permanent magnet, Rev. Sci. Instrum. 55, 449-456, 1984.

2.45 GHz. It follows from equation (2) that the flux density B of the magnetic field in the source must be equal to about 0.0875 T (tesla). This field is excited by a permanent magnet (not shown in the drawing). This means that it is difficult to adjust the strength of the magnetic field to the microwave frequency. The energy is transferred from the microwave circuit to the plasma by a T-shaped antenna.

Because of the relatively low energy of the electrons, most of the ions produced are singly charged. An advantage is that the spread of energy in the ion beam is small, since the source does not contain an electrostatic field. The source is only suitable for the ionization of gases and gives a relatively large ion current, e.g. 400 μA of O_2^+ ions.

Examples of ion implantation

Implantation of oxygen in silicon

The implantation of a high dose of oxygen ions — up to 3×10^{18} cm^{-2} — at a fairly considerable depth in a single-crystal silicon slice makes it possible to produce 'buried' SiO_2 layers. If the dose is not too high, the surface layer is more or less undisturbed since E_l for O^+ ions in silicon is only about 30 keV; see fig. 2. It is therefore possible to produce integrated circuits at the surface on an insulating substrate. The transistors of such a circuit on an insulating substrate interfere with one another less, are faster, and are also less sensitive to cosmic or other radiation.

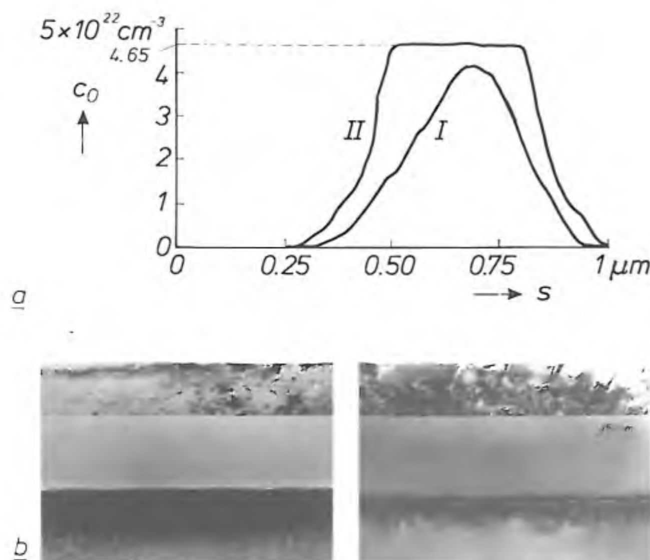

Fig. 13. *a*) The concentration c_O of oxygen in silicon as a function of the depth s below the substrate surface. The curves show that the implantation of oxygen in silicon produces a 'buried' SiO_2 layer as soon as the relative oxygen concentration reaches the stoichiometric value of 66.7 at.%, which corresponds to $c_O = 4.65 \times 10^{22}$ cm^{-3}. Curve I corresponds to a dose of 1.5×10^{18} cm^{-2} and curve II corresponds to 2.5×10^{18} cm^{-2}. The curves are the result of measurements by the HEIS method (High-Energy Ion Scattering)[11]. *b*) Micrographs made with a Philips EM400T transmission electron microscope of cross-sections of a silicon slice with a buried SiO_2 layer: on the left with no annealing, on the right after annealing for two hours at 1200 °C. The second layer is always the amorphous SiO_2 layer. The surface is at the top and is a (100) plane of the original silicon crystal.

We have used a microwave source to implant O_2^+ ions at an energy of 600 keV in silicon. During the implantation the sample was heated to a temperature of 500 to 600 °C. This high temperature ensured that the top layer did not become amorphous and that the surplus of oxygen ions could diffuse away upwards or downwards. *Fig. 13a* shows that as a result of this diffusion the relative oxygen concentration does not continue to increase after the stoichiometric value corresponding to SiO_2, 66.7 at.%, has been reached. The total quantity of implanted oxygen ions thus determines the thickness of the SiO_2 layer produced. After the implantation an annealing treatment is necessary to remove local oxygen precipitates from the upper layer and to correct for lattice damage. Fig. 13*b* shows cross-sections of the sample before and after annealing at about 1200 °C for 2 hours.

Implantations in metals

As noted, the properties of a metal surface can be improved by implanting ions. Hardness, wear resistance or resistance to corrosion can be improved in this way. We have improved the corrosion resistance of copper by implanting aluminium ions. We used a hollow-cathode source that supplied Al^+ ions with a maximum dose of 5×10^{17} cm^{-2} at an energy of 170 keV.

The copper samples were subjected to a corrosion test to IEC 68243 KD. At a temperature of 300K treated and untreated specimens were exposed to air containing 15 ppm of H_2S, at a relative humidity of 75 %. After 8 hours the untreated copper was found to have about 50 times the corrosion of the treated samples.

Fig. 14 shows the results of Auger analyses of the treated copper surface after the corrosion test. Presumably the implanted aluminium was first oxidized to Al_2O_3, and the copper at the surface to Cu_2O. The Cu_2O is converted to Cu_2S. The Al_2O_3 layer finally prevents further corrosion.

[9] R. S. Muller and T. I. Kamins, Device electronics for integrated circuits, Wiley, New York 1984, p. 374;
S. M. Sze (ed.), VLSI technology, McGraw-Hill, New York 1983, p. 483;
W. G. Gelling and F. Valster, The new centre for submicron IC technology, Philips Tech. Rev. 42, 266-273, 1985/86.

[10] R. D. Rung, C. J. Dell'oca and L. G. Walker, A retrograde p-well for higher density CMOS, IEEE Trans. **ED-28**, 1115-1119, 1981.

[11] D. Pramanik and M. I. Current, MeV implantation for silicon device fabrication, Solid State Technol. 27, No. 5 (May), 211-216, 1984;
C. McKenna, C. Russo, B. Pedersen and D. Downey, Applications for MeV ion implantation, Semicond. Int. 9, No. 4 (April), 101-107, 1986.

[12] J. Hilibrand and R. D. Gold, Determination of the impurity distribution in junction diodes from capacitance-voltage measurements, RCA Rev. **21**, 245-252, 1960.

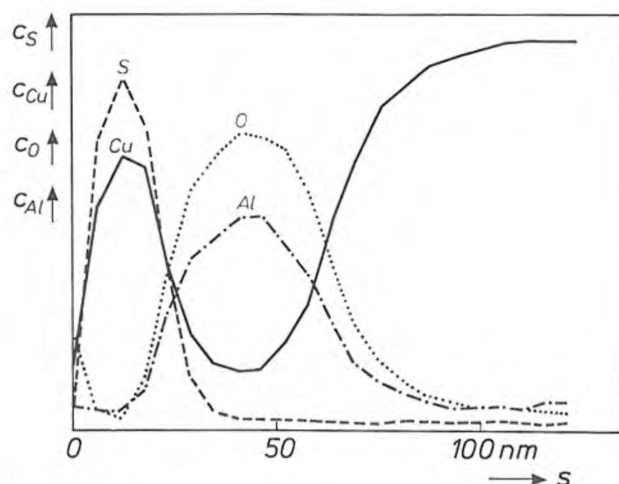

Fig. 14. Results of Auger analyses of a copper sample in which aluminium has been implanted to improve the corrosion resistance. After the implantation the sample was subjected to a corrosion test with H_2S gas and humid air. The scales for the concentrations c_S, c_{Cu}, c_O and c_{Al} of the four different elements in the sample are not comparable. The only known value is $c_{Cu} = 100\%$ for a depth s greater than 100 nm. Before the corrosion test the maximum relative value of c_{Al} was approximately 25 at.%.

High-energy implantations of phosphorus in silicon

In CMOS technology the normal practice for making 'wells' in the substrate [9] is to use low-energy ion implantation followed by drive-in annealing. The annealing enables the atoms of the implanted element to diffuse more deeply into the substrate. Disadvantages of this procedure are that lateral diffusion occurs, the heat treatment takes a good deal of time and it is only possible to obtain profiles whose concentration decreases with depth. What are wanted in the substrate, however, are wells in which the donor or acceptor concentration increases with depth, reaches a maximum and then decreases rapidly. Wells with a concentration profile of this type are called 'retrograde wells' [10]. They can be made by means of high-energy implantations. In CMOS circuits formed from retrograde wells the resistivity at the bottom of the wells is lower, so that there are fewer rejects due to 'latch-up' — a kind of short-circuiting caused by the formation of parasitic thyristors via the substrate.

Almost any shape of concentration profile can be obtained by combining implantations of different dose and energy [11], so that the concentration profiles of the separate implantations are added together. In this way the particular profiles can be made that will ensure the best possible operation of the components of the integrated circuits. To obtain more information about such multiple implantations we have carried out a number of implantations at different energies and measured the corresponding concentration profiles. These were implantations of phosphorus in silicon at energies of 200 to 1400 keV, in steps of 200 keV. Up to 800 keV we used P^+ ions and above it we used P^{++} ions. *Fig. 15* shows the results. The profiles were determined by means of the capacitance-voltage (CV) method [12].

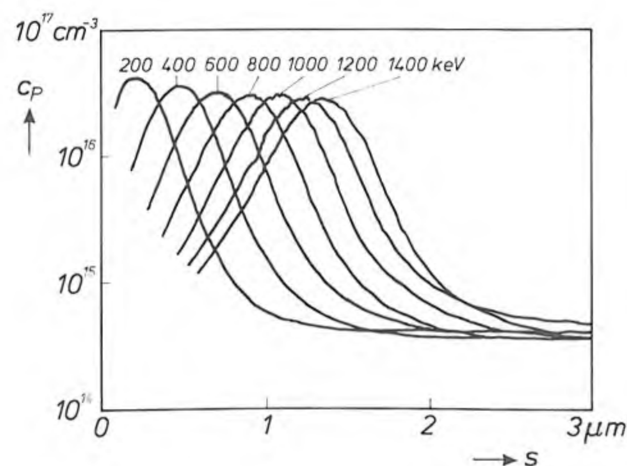

Fig. 15. Result of concentration-profile measurements made by the CV method[12]. The concentration c_P of phosphorus implanted in silicon is plotted as a function of the depth s. The different curves correspond to implantation energies from 200 to 1400 keV. Virtually any implantation profile can be obtained by combining a number of these or other curves.

Summary. Since the high-voltage section of the ion-implantation machine developed at Philips Research Laboratories is not insulated by gas under pressure in a tank, changing the ion source is relatively easy. The machine is therefore particularly suitable for research. The accelerating voltage is high, 800 kV, so that heavy elements can be implanted in heavy substrates. There are two target chambers, one designed for treating silicon slices for IC manufacture, the other designed for other samples, including metals. Implantations in metals can improve properties such as hardness or resistance to corrosion. The half-width of the beam cross-section and the location of the pattern of the beam scan on the sample are evaluated with the aid of a wire frame around the sample; the wire frame is earthed through a milliammeter. The implantation dose is measured with a Faraday cup. Five ion sources have been tested: the hollow-cathode source, the Penning source, the radial-extraction Penning source, the sputter source and the microwave source. Some examples are given to demonstrate the usefulness of the machine: implantation of buried oxygen layers in a silicon slice, implantation of aluminium to improve the corrosion resistance of copper, and the determination of a number of concentration profiles for phosphorus in silicon at different energies.

 Philips Tech. Rev. 43, No. 7, 180-182, July 1987

A laser-Doppler displacement meter

R. J. Asjes, C. S. Caspers and C. H. F. Velzel

In the manufacture of products such as wire, textiles or paper the moving length of material can be measured by pressing a runner wheel with a revolution counter against the surface of the moving material. This widely used method has its problems, however. The runner wheel can easily slip, resulting in an inaccurate measurement, and the material may be damaged by the wheel, which has to be in contact with it.

At the Philips Centre for Manufacturing Technology a displacement meter based on the laser-Doppler principle has now been developed. The instrument can be used for measuring displacements of widely diverse materials without being in contact with the material and with an error of less than 0.2%. Before looking more closely at the instrument itself, we shall first touch briefly on the laser-Doppler principle.

When a laser beam is split into two beams that are made to intersect, an interference pattern is produced in the intersection volume; see *fig. 1*. This interference pattern consists of light and dark planes, parallel to the 'optical axis' and perpendicular to the plane of the drawing. A small particle moving through the intersection volume passes through alternate light and dark planes. When it passes through a light plane it will scatter light, but not when it passes through a dark plane. If δ is the distance between the successive light planes, and v_p is the velocity of the particle perpendicular to the planes, intensity variations in the scattered light can be observed, with a frequency

$$f_D = \frac{v_p}{\delta}. \qquad (1)$$

The principle of a laser-Doppler velocity measurement is that the frequency f_D is measured and the velocity v_p is calculated: the distance δ can be calculated from the geometry of the configuration and the wavelength of the laser light.

In the situation shown in fig. 1 the detector has to have a very wide frequency range, since a high velocity implies a high frequency and a low velocity a low frequency. At very low velocities this can present problems. The difficulty can be overcome, however, by arranging for the planes of the interference pattern to move at a constant velocity v_g. If we assume that the direction of v_g is opposite to that of v_p, then the frequency of the intensity variations is

$$f_m = \frac{v_p + v_g}{\delta} = f_D + f_g, \qquad (2)$$

where f_m is the modulation frequency observed, v_p is the velocity of the particle, f_D is the Doppler frequency corresponding to the velocity v_p given by Eq. (1), and f_g is the frequency observed when $v_p = 0$. In this way, intensity variations (at a frequency f_g) are also observed when the particle itself is stationary, as the interference planes 'pass over it'. The interference pattern can be made to move by using a circular grating as the beam splitter. (The lines of such a grating are arranged radially around the circumference of a disc.) If the grating is rotated at a constant angular velocity, the planes in the interference pattern will also move at a constant velocity [1]. When the interference planes move in the opposite direction to the particle, the frequency observed increases in proportion to the increase in the velocity of the particle. In reality, of

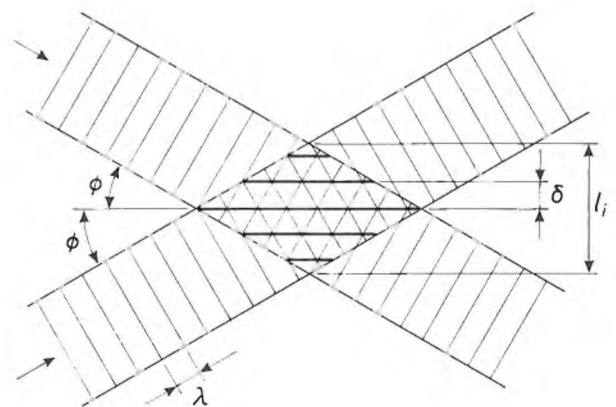

Fig. 1. The interference pattern obtained by splitting a laser beam into two beams and then making them intersect. The pattern consists of light and dark planes perpendicular to the plane through the two beams. If λ is the wavelength of the laser light and ϕ the angle between either beam and the optical axis, then the distance δ between the two maxima in the interference pattern is $\delta = \lambda/(2 \sin \phi)$. The length of the interference pattern in the direction of the velocity and length measurement is l_i.

Ir R. J. Asjes, Ing. C. S. Caspers and Dr Ir C. H. F. Velzel are with the Philips Centre for Manufacturing Technology (CFT), Eindhoven.

course, there will not be just a single particle, but the surface of something like a cable or a wire, for example. Such a surface will almost invariably contain enough small asperities to represent a stream of particles whose mean velocity is measured.

As appears from Eq. (2) either f_m or f_g can be kept constant. Usually it is preferable to keep f_g constant [1]. This can be done by rotating the circular grating at a constant angular velocity. When the velocity v_p changes, so too does the observed frequency f_m. We have preferred, however, to keep f_m constant (at least approximately) [2]. This is done by controlling the angular velocity of the grating — and hence f_g — so that f_m always has about the same value. In this way, velocity and displacement can be determined in principle from the angular velocity of the grating, which is continuously measured by tachogenerator (we shall return to this presently). Some calculation is still necessary, however, since we do not keep f_m exactly constant. If we did, it would be only be necessary to measure f_g to determine v_p. However, keeping f_m accurately constant would require an extremely refined control system. Keeping f_m only approximately constant means that the bandwidth of the processing electronics can be much smaller, and the velocity can be calculated very accurately from the two measured values of f_m and f_g.

We shall now look briefly at the mechanical part of the instrument (the 'measuring head') before dealing with the electronics in more detail.

The light source of the instrument (see *fig. 2*) is an HeNe laser with a radiated power of about 2 mW at a wavelength of 632.8 nm. The laser beam is focused on the rotating grating, and an image of the grating is produced on the moving surface of the object by the objective. Between the grating and the objective there is a diaphragm with two apertures, which passes only the two first-order beams and stops those of higher order. The light scattered by the object is focused on the detector, a silicon P-I-N diode, by a condenser, which consists of a combination of two plastic Fresnel lenses. These have a large diameter (so that they intercept much of the scattered light), and they are flat, light and inexpensive. Each lens has two holes for the two beams to pass through; the detector is mounted between the two beams. The optical system described here contains a minimum of optical components. The focusing lens and the objective must have good imaging characteristics and can be relatively small (about 2 cm). The condenser, on the other hand, does not need to have such good imaging characteristics but it does have to be relatively large (about 10 cm), as we noted earlier. It is therefore convenient to use different lenses for objective and condenser. (The same

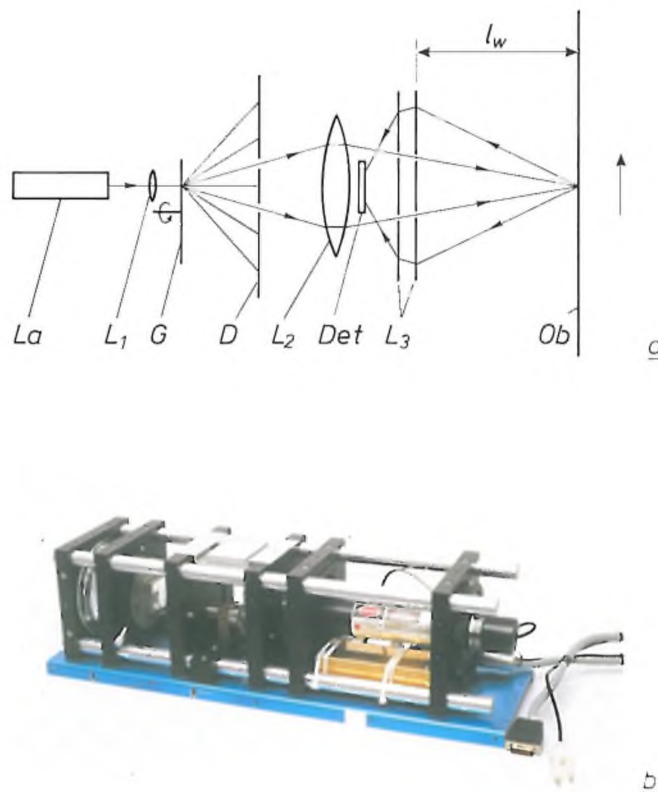

Fig. 2. *a*) Diagram of the 'measuring head' of the displacement meter. *La* HeNe laser. L_1 focusing lens. *G* rotating grating. *D* diaphragm that passes only first-order beams. L_2 objective lens. *Det* detector. L_3 condenser, consisting of two Fresnel lenses. *Ob* object whose displacement is to be measured. l_w distance between the front of the measuring head and the object (working distance). *b*) Photograph of the measuring head. All the components are contained in square mounts connected to each other by four steel rods. The cylindrical laser is on the right between the rods; the Fresnel lens can just be seen on the left.

lens is often used for both functions, which makes the optics fairly expensive since a large lens with good imaging characteristics is required.) All the components are contained in a 'measuring head', made from components of a commercially available assembly system.

The electronic processing of the signal will be explained with the aid of the simplified diagram in *fig. 3*. The detector signal is fed to a preamplifier and a filter that passes frequencies between 420 kHz and 485 kHz. The signal passed by the filter is converted by a pulse shaper into a binary signal that drives a phase-locked loop consisting of a mixer (in our case an exclusive OR gate), a switch, an integrator and a voltage-controlled oscillator. The amplitude of the input signal of the pulse shaper is used for keeping the switch in the

[1] J. Oldengarm, Development of rotating diffraction gratings and their use in laser anemometry, Opt. & Laser Technol. 9, 69-71, 1977.

[2] The idea of keeping the modulation frequency constant is due to M. P. Weistra of Philips Research Laboratories, Eindhoven; see Netherlands patent application No. 8301917, 31 May 1983.

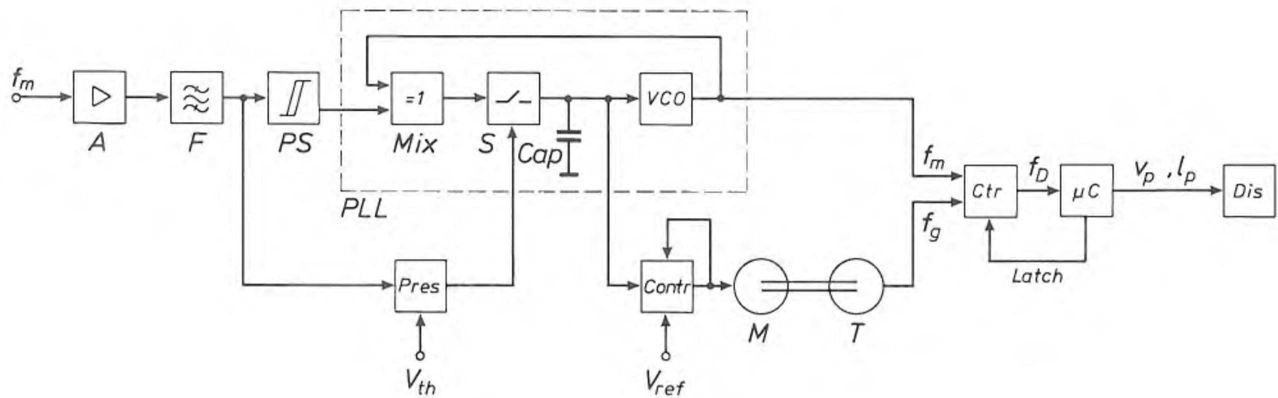

Fig. 3. Simplified block diagram of the signal-processing electronics, described in the text. f_m frequency of the input signal. *A* preamplifier. *F* bandpass filter. *PS* pulse shaper. *Mix* mixer (here an exclusive OR gate). *S* switch. *Cap* capacitor (integrator). *VCO* voltage-controlled oscillator. *Mix*, *S*, *Cap* and *VCO* form the phase-locked loop *PLL*. *Pres* circuit for checking whether the amplitude of the input signal is smaller than the threshold voltage V_{th}. If it is, *S* is opened. *Contr* control circuit for the motor that drives the grating. V_{ref} reference voltage. *M* motor for the grating. *T* tachometer. f_g frequency of the interference-pattern movement. *Ctr* difference counter. *latch* counter-latching device. f_D Doppler frequency corresponding to the velocity v_p (given by Eq. 1). μC microcomputer. *Dis* display panels that display the measured velocity v_p and the displacement l_p.

phase-locked loop closed. When the amplitude of the detector signal falls below a threshold value V_{th}, e.g. if the signal is interrupted, the switch opens and the voltage-controlled oscillator continues to oscillate for about a second. In this way the system is protected from short interruptions. The input voltage of the oscillator is compared with a reference voltage V_{ref}; the difference voltage is used for driving the grating motor. The effect of this is to limit the frequency of the detector signal to a band of a few kHz about a mean value of 455 kHz, which makes the analog part of the circuit considerably simpler [2]. The output signal of the phase-locked loop consists of pulses at the frequency f_m. The frequency f_g at which the interference pattern moves is obtained from a tachometer mounted on the shaft of the motor that drives the grating. The pulse trains from the phase-locked loop and the tachometer are fed to a latched difference counter. A microcomputer determines the sampling time t_s (in our case 1/800 s) in which the frequencies f_m and f_g are subtracted one from another. After a time t_s the contents of the counter amount to $(f_m - f_g)t_s = f_D \times t_s$. As this value is latched after each sampling interval, it is available for the microcomputer during the next sampling interval. The computer applies a calibrating factor, to give $f_D \times t_s$ directly as the mean velocity over the sampling interval that has just elapsed. It also counts the successive values of $f_D \times t_s$ during a period of time, to give the displacement that has occurred during that time.

It can be shown by error analysis that the inaccuracy of the result of the measurement is about 0.03% when the velocity of the object is constant [3]. If it is not constant, an absence of signal (e.g. because of a brief interruption of one of the two light beams) can introduce an error in the measured displacement. However, if the signal is present for 90% of the time, the standard error is still less than 0.2% — much less than with conventional methods of displacement measurement. The principal data of the instrument are listed in *Table I*.

Table I. Some numerical data for the displacement meter. The symbols are explained in figs 1 and 2.

Maximum measurable displacement	16 km
Maximum measurable velocity	12 m/s
δ	0.02 mm
l_i	1 mm
l_w (minimum)	60 mm
l_w (maximum)	75 mm

[3] C. H. F. Velzel, Laser Doppler displacement meter with controlled grating speed, Proc. Int. Conf. on Optical techniques in process control, The Hague 1983, pp. 289-294.

1937 THEN AND NOW 1987

Measuring instruments

By 1937 there was already a need for an easily operated test set that could be used for various electrical measurements on devices such as 'wireless valves' (photo lower right) [*]. The operation of the test set was substantially automated by using a contact bridge with 140 contacts. Inserting the 'code card' for a particular valve (photo lower centre) set the instrument up correctly in a single operation. Certain effects such as short-circuits between electrodes or a broken filament were indicated by signal lamps; other characteristics could be read from a milliammeter with its scale divided into two regions: blue for 'pass', red for 'fail'.

In 1987 instruments generally contain the most modern electronic components such as memories and microprocessors. Our example is the highly advanced PM 3320 digital storage oscilloscope (large photo). This instrument can be used for measuring analog signals with a bandwidth of no less than 200 MHz. It does so with the aid of P^2CCD memories [**] and analog-to-digital conversion with an accuracy of 10 bits. The oscilloscope also includes a memory that will store more than 4×4000 measured values. Mathematical manipulations, such as the multiplication of two signals, can be performed before display on the screen (10 cm × 12 cm). If the two signals represent current and voltage, for example, a curve representing the instantaneous power is obtained. The number of controls is kept as small as possible by introducing eight variable-function 'soft keys' next to the screen (photo lower left). The actual functions in use are shown on the screen. Without this facility the PM 3320 would need more than 100 controls. The complete setting-up routines for certain frequently made measurements can also be stored in the memory of the instrument, so that it can be set up instantaneously at the touch of a key.

[*] From Philips Technical Review, February 1937.

[**] See also H. Dollekamp, L. J. M. Esser and H. de Jong, P^2CCD in 60 MHz oscilloscope with digital image storage, Philips Tech. Rev. 40, 56-68, 1982.

Philips Tech. Rev. 43, No. 7, 184-191, July 1987

Quantitative measurements by the Schlieren method

G. Prast

In many different areas of technology the tolerances for the dimensions of parts and components are very strict. This means that inaccuracy of form and surface roughness must be as low as possible. Checking workpieces for these requirements can be difficult and sometimes it can only be done in the laboratory. In production conditions the Schlieren method may provide the answer. The combination of digital computation with this originally qualitative method from the last century allows us to use it for quantitative measurements.

Roughness and shape of surfaces

With the growing importance of optics — in the storage and exchange of digital information, for example — optical components such as mirrors and lenses will make an even greater contribution to Philips products than in the past. The specifications for the shape and surface roughness of lenses and mirrors are extremely demanding. The shape of the aspheric objective lens in the tracking mechanism of a LaserVision or Compact Disc system — a lens that can take the place of a system of four spherical lenses for reading out the information on a Compact Disc — must not differ from the standard by more than 0.1 μm. Obviously, it only makes sense to manufacture these extremely precise optical components if we can find out whether the product meets the specifications. The moulds for pressing the lenses can be made with the COLATH high-precision lathe [1]. The normal practice so far has been to inspect the optical components afterwards. A number of optical components are then assembled to form a unit that must satisfy some easily checked criteria. This 'post'-inspection can mean that the moulds have to be machined once again. It is better to have a method that can be used to assess the quality of the mould when it is being made. If such a method can also be performed on the lathe itself, any errors can be corrected immediately, without the need for repeated setting up, which can introduce new errors. Making optical components is only one use of this high-precision machining technique, of course. The specifications for the shape and roughness of machined surfaces for other purposes may be just as strict.

Two types of measurements are widely used for determining the shape and roughness of surfaces: mechanical methods and optical methods. In the mechanical methods of measurement a thin stylus is moved at constant velocity over the surface. During the movement the stylus is pressed lightly against the surface so that it follows its contours. The movement of the stylus perpendicular to the surface is measured and gives the roughness and shape of the surface. The mechanical methods have their disadvantages: they are time-consuming, sensitive to vibrations and cannot be used for all materials because of the direct contact between stylus and surface. Nor are they very practical for inspection during production, because the workpiece usually has to be moved elsewhere for the measurement.

The optical methods of measurement do not have the disadvantage of direct contact between workpiece and measuring device. This category includes light-scattering methods, interference methods and the Schlieren method. The Schlieren method is an example of an originally qualitative method that has since

Ir G. Prast is with Philips Research Laboratories, Eindhoven.

been made quantitative by using modern equipment and digital signal processing, so that it can easily be used in production conditions. In this article we shall look first at the principle of the method and then discuss its application in a special type of microscope.

Principle of the Schlieren method

The method was introduced in the middle of the last century by J. B. L. Foucault as a way of checking the quality of large astronomical mirrors. A few years later A. Töpler discovered a new application: studying inhomogeneities in the flow of gases, e.g. in wind tunnels. It was this application that gave the method its name. A 'Schliere' or 'streak' is a thin zone of locally different refractive index in a transparent object. Light incident on the Schliere emerges in a different direction from the direction it would take in the absence of any such inhomogeneity. The change in direction is a measure of the inhomogeneity (or of the irregularity in the surface of an object if the light is reflected). A purely qualitative observation of a number of inhomogeneities in the refractive index of air can be seen in *fig. 1*.

Fig. 1. This picture, made by the Schlieren method, shows a bullet travelling through the air above two candle flames. This photograph is taken from the book of note [2] (page 560).

Differences in the refractive index of parts of a transparent object are not always easy to observe. It is possible, however, to enhance the contrast between light beams that pass through parts of the object with different refractive indices. This is done by screening off a part of each light beam emerging from the object [2]. *Fig. 2* shows the principle of the method. Lenses L_1 and L_2 produce an image of the light source B, and lenses L_2 and L_3 produce an image of the object O on the screen S. Part of the beam is screened off by the knife-edge K at the point where the image of the source is formed. The 'Schliere' is therefore shown on the screen as a streak that is more brightly illuminated than the background, since a smaller part of the beam from the 'Schliere' is intercepted by the knife-edge, as compared with neighbouring locations. In this example the object is transparent, but the same measurement method can of course be used with a reflecting object. Light source and screen are then situated on the same side of the object.

By measuring the light intensity (illuminance) on the screen the location of any inhomogeneity in the object or of any irregularity on its surface can be determined. Originally this method was mainly qualitative, but now that accurate photodiodes are available (in our configuration we use a row of 1024 CCD photodiodes with dimensions of $13\,\mu m \times 13\,\mu m$ on a single chip), and large amounts of measured data can be processed rapidly by computer, quantitative measurements are possible.

In the remainder of this section we shall derive these quantitative results. We shall initially assume that we have a configuration with ideal optical components. Later we shall see that errors that arise because these components are not ideal can be eliminated by using differential measurements.

Configuration with ideal optical components

In the arrangement shown in fig. 2, L_1 is an optically perfect lens and B is a light source that illuminates the object plane uniformly. A planar wavefront is incident on the object. If we assume that the gradient in the optical pathlength s_{opt} through the object at position P is $\partial s_{opt}/\partial x$, then the wavefront, which was truly planar before it met the object, will have a corresponding local deviation. There can be two reasons for a gradient in the optical path through the object. The refractive index in the object may differ from point to

[1] J. Haisma, W. Mesman, J. M. Oomen and J. C. Wijn, Aspherics, III. Fabrication, testing and application of highly accurate aspheric optical elements, Philips Tech. Rev. 41, 296-303, 1983/84.

[2] H. Wolter, Schlieren-, Phasenkontrast- und Lichtschnittverfahren, in: S. Flügge, Handbuch der Physik, Bd. 24, Springer, Berlin 1956, pp. 555-645.

point, or the object may be thicker or thinner in some places. If it is thicker or thinner the relation between the gradient in the object and the deviation in the shape of the wavefront can be explained in the following way. Consider an object of the shape shown in *fig. 3*, with a planar wavefront *WF* incident on it at time t. The position of the wavefront is indicated at a number of times separated by a fixed interval Δt. In equal intervals Δt the wavefront travels identical optical pathlengths. (The optical pathlength is the product of distance and refractive index.) The object is made of a material with a refractive index n higher than that of the surrounding air. The velocity of the wavefront in the object is $1/n$ times the velocity in air. Consequently, at positions where the object is thinner the wavefront reaches the position $z = d$ earlier. The distance the wavefront has travelled at $x = 0$ between $t + \Delta t$ and $t + 3\Delta t$ is exactly equal to the thickness d of the object. At $x = \Delta x$ this distance is $d + \Delta d$. The time $2\Delta t$ (the distance travelled divided by the velocity of the wavefront) is equal to $d/(c/n)$ and also to $\Delta z/c + (d - \Delta z)/(c/n) + \Delta d/c$. The distance Δd by which the wavefront at the position Δx is 'ahead of' the wavefront at $x = 0$ is therefore $\Delta d = \Delta z(n - 1)$. The tangent of the angle α between the wavefront and the z-axis is:

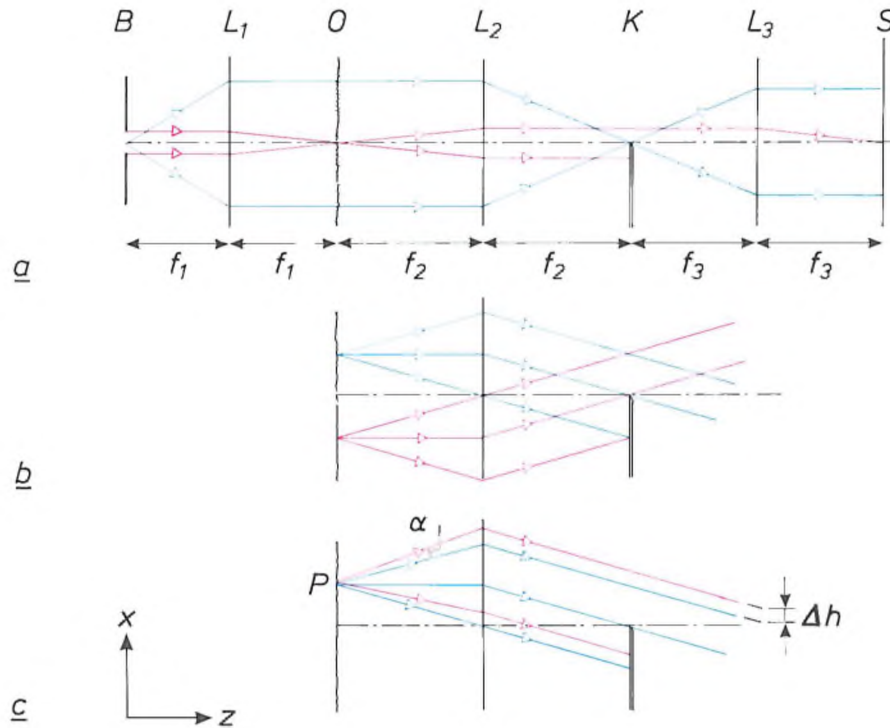

Fig. 2. *a*) Example of a configuration for the Schlieren method. An image of a rectangular light source B is formed by two lenses (L_1 and L_2 with focal lengths f_1 and f_2) at the focal plane of the second lens (blue beam). Between L_1 and L_2 there is a transparent object O. An image of the object is produced on the screen S by the lenses L_2 and L_3 (red beam). At the focus of the second lens there is a knife-edge K. The coordinate perpendicular to the knife-edge is x, and z indicates the direction perpendicular to the object. *b*) Half of a light beam originating from an arbitrary point P of the object is screened off by the knife-edge. *c*) If there is an inhomogeneity in the object at the position P, a light beam is deflected through an angle α. The result is that less than half of the beam originating from P is screened off by the knife-edge. The image of the light source produced at the focal plane of the second lens by the light incident on the object through point P is displaced by a distance Δh. The inhomogeneity is visible on the screen as a streak brighter than its surroundings.

$$\tan \alpha = \frac{\Delta d}{\Delta x} = \frac{\Delta z(n - 1)}{\Delta x}.$$

If ϕ is small — the Schlieren method can only be used if it is — then α is also small and we therefore have:

$$\alpha = \frac{\Delta z(n - 1)}{\Delta x}.$$

The deflection of the light rays, which are perpendicular to the wavefronts, is therefore proportional to the ratio $\Delta z/\Delta x$, which is equal to the gradient $\partial z/\partial x$ in the limit for small distances.

At the focal plane of L_2 the image formed of the light source by light rays passing through point P is

displaced by a distance $\Delta h = \alpha f_2$. This implies that the intensity of the light passing the knife-edge increases because of this gradient. With no gradient the light intensity (I_0) is proportional to $\frac{1}{2}h$, whereas with a gradient ($I_0 + \Delta I$) it is proportional to $\frac{1}{2}h + \Delta h$, where h is the dimension of the image of the light source. The relative increase in intensity at the screen as a result of the gradient is

$$\frac{\Delta I}{I_0} = \frac{\Delta h}{\frac{1}{2}h} = \frac{\alpha f_2}{\frac{1}{2}h} \quad \text{or} \quad \alpha = \frac{h\,\Delta I}{2 f_2\, I_0}. \tag{1}$$

The gradient can thus be directly determined from the measured relative increase in intensity.

The sensitivity of the method is

$$\frac{\mathrm{d}\Delta(I/I_0)}{\mathrm{d}\alpha} = \frac{2f_2}{h} = \frac{2f_1}{l}, \tag{2}$$

where $h = (f_2/f_1)l$, with l the dimension of the light source perpendicular to the optical axis and perpendicular to the edge. By increasing f_1 or reducing l the sensitivity of the method can be increased, within certain limits. The sensitivity cannot be increased indefinitely, however, because the measurement range also depends on these two quantities. If $\Delta h = \alpha f_2 > \frac{1}{2}h$, the image is either fully illuminated or fully blacked out and the image intensity is no longer linearly dependent on the gradients. In addition, diffraction effects become significant if the dimensions of the light source become too small.

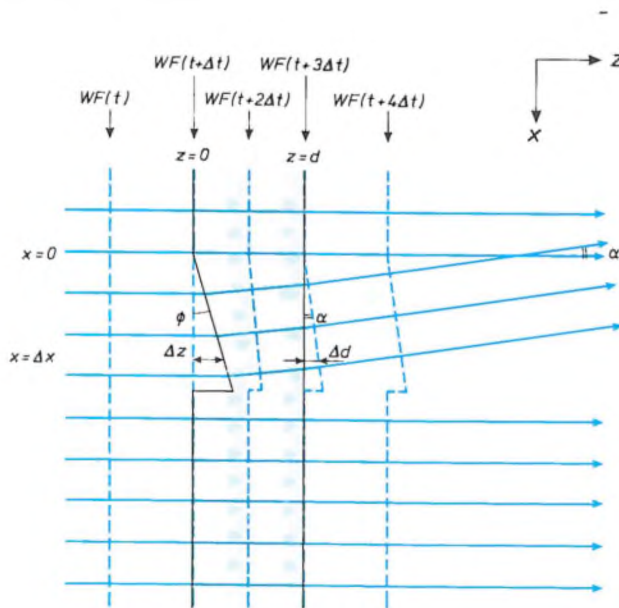

Fig. 3. The relation between the gradient in the optical path and the perturbation of the wavefront. The grey area represents part of a transparent object of thickness d, in which a wedge-shaped piece (with an apex angle ϕ) is missing. A plane wavefront WF is incident on the object from the left at time t_1. The position and shape of the wavefront are shown at a number of times t_1 to t_6 at intervals of Δt. The blue continuous lines represent the light rays, which are perpendicular to the wavefronts. At the height of the wedge the light rays leave the object at an angle α.

Configuration with real optical components

The above argument only applies for perfect optical components and uniform illumination of the object. In reality, neither condition can be satisfied. Nevertheless the Schlieren method remains useful because these drawbacks can be overcome by making four measurements of the light intensity on the screen S: with and without a knife-edge and with and without an object.

The intensity without knife-edge and without object is given by:

$$I_0' = c_{x,y} h b, \tag{3}$$

where $c_{x,y}$ is the position-dependent illumination of the plane where the object will be located, and h and b are the height and width of the image of the source that will be produced at the knife-edge. Next, the knife-edge is introduced in such a way that the actual edge is situated on the optical axis of the configuration. Owing to imperfections in the positioning of the lenses, however, the centre of the image does not lie exactly on the edge but is separated from it by a distance $\xi_{x,y}$. With a knife-edge and without object the intensity is:

$$I_0 = c_{x,y}(\tfrac{1}{2}h + \xi_{x,y})b. \tag{4}$$

The knife-edge is then removed and the object put in its place. The intensity with object and without knife-edge is:

$$I' = c_{x,y} h b T_{x,y}, \tag{5}$$

where $T_{x,y}$ is the transmittance of the object. Finally the intensity is measured with both knife-edge and object present:

$$I = c_{x,y}(\tfrac{1}{2}h + \xi_{x,y} + \alpha_{x,y} f) b T_{x,y}, \tag{6}$$

where f is the focal length of the second lens. We now have two relative measurements of the light intensity: I_0/I_0' measured without an object and I/I' measured with an object. The difference $M_{x,y}$ between these measurements is:

$$M_{x,y} = \frac{I}{I'} - \frac{I_0}{I_0'} = \frac{c_{x,y}(\frac{1}{2}h + \xi_{x,y} + \alpha_{x,y} f) b T_{x,y}}{c_{x,y} h b T_{x,y}} - \frac{c_{x,y}(\frac{1}{2}h + \xi_{x,y}) b}{c_{x,y} h b} = \frac{\alpha_{x,y} f}{h}. \tag{7}$$

Between $M_{x,y}$ and $\alpha_{x,y}$ we therefore find a simple relation in which a correction is made not only for the imperfections of the lenses and the source but also for different diode sensitivities. The only requirement for the diodes is that they should produce a signal that is proportional to the incident light intensities. The measurements without an object are in effect a cali-

bration of the measurement configuration and only have to be made once.

The Schlieren microscope

The Schlieren method is a useful means of measuring thickness differences and refractive-index variations in transparent objects. The principle can also be applied successfully in a microscope. This is not self-evident, because in deriving the quantitive method we used geometrical optics, which cannot always be used directly for the theory of image formation in a microscope.

It is possible to make f_2 and f_3 in fig. 2 large so as to obtain a high magnification. For example, with $f_2 = 30\,\text{mm}$ and $f_3 = 400\,\text{mm}$ we obtain a magnification of 13 times. With the diode dimensions of $13\,\mu\text{m} \times 13\,\mu\text{m}$ we thus look at 'points' in the object of $1\,\mu\text{m} \times 1\,\mu\text{m}$. We have then in fact made a microscope. However, we shall have to show in another way that the linear relation between the light intensity in the image and the gradient at the corresponding point in the object, as derived by geometrical optics, is preserved. This can be done by applying Abbe's calculation of image formation in the microscope to the case where half the diffraction pattern formed at the back focal plane of the objective lens (the Fourier plane) is covered and the image is formed by the uncovered half. From the calculation given below it will be seen that the Schlieren theory remains valid as long as the diffraction orders in the Fourier plane overlap [3].

This condition can be derived as follows. A microscope forms an image of a reflecting object with a surface whose height follows a sine function: $z = z_0 + \frac{1}{2}\Delta z \cos \Omega x$, where Ω is the spatial frequency of the irregularity, z the coordinate parallel to the optical axis and x is the coordinate perpendicular to the optical axis and perpendicular to the knife-edge. An incident plane wave $E = E_0 \cos(\omega t - kz)$, where E is the amplitude and k the circular wave number, is reflected:

$$\begin{aligned} E &= E_0 \cos(\omega t + kz_0 + k\Delta z \cos \Omega x) \\ &= E_0 [\cos(\omega t + kz_0) \cos(k\Delta z \cos \Omega x) \\ &\quad - \sin(\omega t + kz_0) \sin(k\Delta z \cos \Omega x)]. \end{aligned}$$

For $k\Delta z \ll 1$ this becomes

$$\begin{aligned} E = E_0 [\cos(\omega t + kz_0) \\ - \tfrac{1}{2} k\Delta z \sin(\omega t + kz_0 + \Omega x) - \tfrac{1}{2} k\Delta z \sin(\omega t + kz_0 - \Omega x)]. \end{aligned} \tag{8}$$

The different terms in this expression represent the orders 0, 1 and -1 of the difraction pattern. At the focal plane of the objective they are imaged as three points spaced by $f\Omega/k$, where f is the focal length of the objective. In reality there is not just a single plane wave incident on the object, but a beam originating from the light source, which has non-zero dimensions. At the focal plane of the objective three images of the light source are formed, as shown in *fig. 4*. Light waves originating from the same point in the light source and reaching the same point in the image via different paths (the different orders) will interfere with each other. The amplitudes of the interfering light waves have to be added. After squaring and integrating over the light source we obtain the intensity pattern of the image.

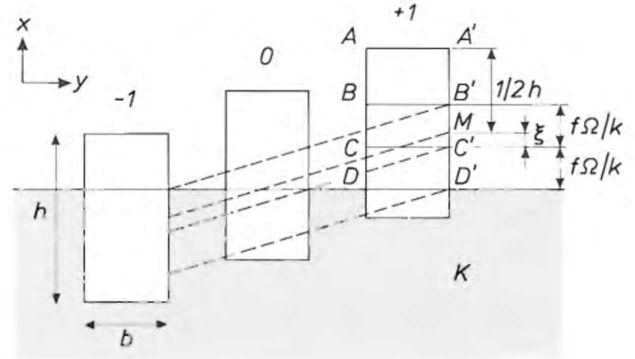

Fig. 4. The location of the diffraction images of order -1, 0 and $+1$ relative to the knife-edge. In fact the three images are only displaced at right angles to the edge, but for clarity they are shown here displaced along the edge as well. M indicates the centre of the image of height h, and C is the position of the knife-edge in the diffraction image. There are three regions: $AA'BB'$, where all three diffraction images pass the knife-edge. $BB'CC'$, where only the zero-order and 1st-order diffraction images pass the knife-edge, and $CC'DD'$, where only the 1st-order diffraction image passes the knife-edge. The images are spaced at a distance $f\Omega/k$.

Since one, two or three diffraction orders may pass the knife-edge, there are three different regions in the diffraction pattern:

- In the region between AA' and BB', where all three orders of the diffraction pattern pass the knife-edge, the amplitude E_{AB} of the wavefront is:

$$E_{AB} = E_0 [\cos(\omega t + kz_0) - k\Delta z \cos \Omega x \sin(\omega t + kz_0)],$$

or

$$E_{AB}^2 = E_0^2 [\cos^2(\omega t + kz_0) - 2k\Delta z \cos \Omega x \sin(\omega t + kz_0) \cos(\omega t + kz_0)],$$

with the condition that $k\Delta z \ll 1$. The surface is given by

$$S_{AB} = [\tfrac{1}{2}h + \xi - f\Omega/k]b,$$

and the total intensity I_{AB} in this region is:

$$I_{AB} = S_{AB} \int E_{AB}^2 \,dt = \tfrac{1}{2} \left[\tfrac{1}{2}h + \xi - \frac{f\Omega}{k} \right] E_0^2\, b. \tag{9}$$

- Next we consider the region between BB' and CC', where only the zero-order and 1st-order diffraction images pass the knife-edge. Here we have:

$$E_{BC} = E_0 [\cos(\omega t + kz_0) - \tfrac{1}{2} k\Delta z \sin(\omega t + kz_0 + \Omega x)],$$

or

$$\begin{aligned} E_{BC}^2 = E_0^2 [\cos^2(\omega t + kz_0) - k\Delta z(\cos^2(\omega t + kz_0) \sin \Omega x \\ - k\Delta z \sin(\omega t + kz_0) \cos(\omega t + kz_0) \cos \Omega x)]. \end{aligned}$$

For the surface of this region $S_{BC} = (f\Omega/k)b$. The total light intensity on this area is:

$$I_{BC} = \tfrac{1}{2} \frac{f\Omega b}{k} E_0^2 [1 - k\Delta z \sin \Omega x]. \tag{10}$$

• Finally, for the region between CC' and DD', where only the 1st-order image passes the knife-edge:

$$E_{CD} = E_0[-\tfrac{1}{2}k\Delta z \sin(\omega t + kz_0 + \Omega x)],$$

or $E^2_{CD} = 0$ and hence also $I_{CD} = 0$.
The total intensity of the light that passes the knife-edge is:

$$I = I_{AB} + I_{BC} + I_{CD}$$

$$= \tfrac{1}{2}\left[\tfrac{1}{2}h - \frac{f\Omega}{k} + \xi + \frac{f\Omega}{k}(1 - k\Delta z \sin \Omega x)\right] E_0^2 b$$

$$= \tfrac{1}{2} E_0^2 b \left(\tfrac{1}{2}h + \xi - f\frac{\partial z}{\partial x}\right), \qquad (11)$$

from which it appears that the image intensity is indeed proportional to the gradient in the refractive index in the object, except for a constant term.

However, if $\frac{1}{2}h + \xi$ is smaller than $(f\Omega)/k$, then light of the diffraction image of order -1 does not pass the knife-edge. We then have $AB = 0$, so that $I_{AB} = 0$ and $BC = \frac{1}{2}h + \xi$. The total intensity is then:

$$I = I_{BC} = \tfrac{1}{2} E_0^2 b (\tfrac{1}{2}h + \xi)(1 - k\Delta z \sin \Omega x). \qquad (12)$$

If we define a critical frequency Ω_{cr} for the spatial frequency of the irregularities on the surface such that light of the image of order -1 only just fails to pass the knife-edge

$$\Omega_{cr} = (\tfrac{1}{2}h + \xi)k/f,$$

or

$$k = \frac{\Omega_{cr} f}{\frac{1}{2}h + \xi}.$$

Then

$$I_{BC} = \tfrac{1}{2} E_0^2 b \left(\tfrac{1}{2}h + \xi - \frac{\Omega_{cr}}{\Omega} f \frac{\partial z}{\partial x}\right). \qquad (13)$$

If the spatial frequency of the irregularities Ω is smaller than Ω_{cr}, then equation (11) applies and the gradient is proportional to the intensity of the image. If this condition is satisfied, the three diffraction images overlap. It is therefore immediately clear that, if the light source is made larger, the condition for ordinary Schlieren calculations is satisfied up to higher frequencies. The critical frequency Ω_{cr} also increases if ξ is made larger. This means that the knife-edge should be adjusted so that part of the image of order -1 passes the knife-edge. If the spatial frequency of the irregularities is greater than Ω_{cr}, then equation (13) applies. There are still intensity differences in the image, but these are no longer proportional to the gradient, since they are attenuated by a factor of Ω_{cr}/Ω with respect to the gradient.

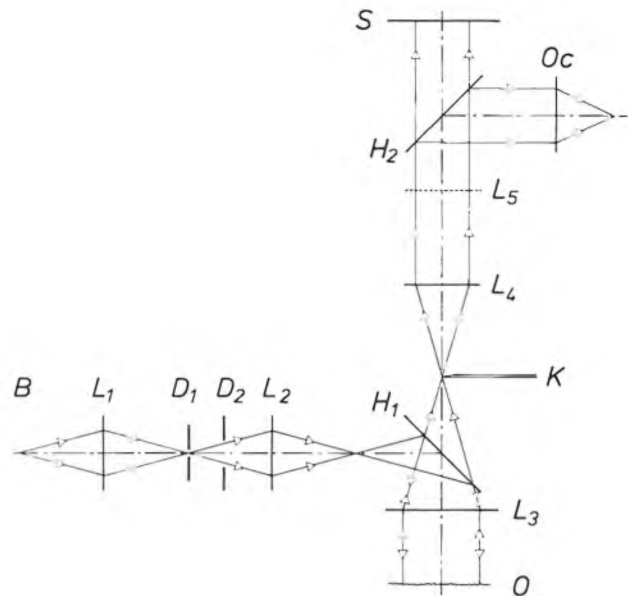

Fig. 5. Principle of the Schlieren microscope. Light from a light source is projected on to the object O by the lenses L_1 and L_2, the diaphragms D_1 and D_2 and the beam-splitter H_1. An image of the source is produced by the objective L_3 at the focal plane, where the knife-edge is located. An image of the object is produced on the diode array S by lens L_4. The second beam-splitter H_2 and the eyepiece Oc are used for focusing at the object. An auxiliary lens L_5 can be used for focusing at the back focal plane of the objective, where the diffraction image can be observed together with the knife-edge.

The distance between the zero-order and 1st-order diffraction images of the source because of periodic irregularities in the object is $d = (\lambda/w)f$, where w is the period of the irregularity and λ the wavelength of the light. The dimension of the image of the source perpendicular to the optical axis is h, so that the Schlieren theory applies when $h > (\lambda/w)f$ or $w/\lambda > f/h$. Irregularities at a small spacing (w small) can be seen if f/h is small. Unfortunately, this ratio also sets a limit to the sensitivity of the method for determining the magnitude of the gradient (see equation 2) and we cannot therefore go on reducing f/h indefinitely. Practical values in such a measurement are $f = 30$ mm, $h = 3$ mm. The intensity $M_{x,y}$ on the screen can be produced with present-day diode arrays to an accuracy $(\Delta M_{x,y})$ of 5×10^{-3}. The intensity is proportional to the gradient in the optical path $\partial s_{opt}/\partial x$, which, for reflecting surfaces, is twice the roughness $\partial z/\partial x$ on the surface:

$$M_{x,y} = \frac{f}{h}\left(\frac{\partial s_{opt}}{\partial x}\right) = \frac{2f}{h}\left(\frac{\partial z}{\partial x}\right).$$

The accuracy to which the height differences on the surface $[\Delta(\partial z/\partial x)]$ can be determined is therefore directly related to the accuracy to which the intensities can be determined:

$$\frac{\partial z}{\partial x} = \frac{h}{2f} M_{x,y},$$

$$\Delta\frac{\partial z}{\partial x} = \frac{h}{2f}\Delta M_{x,y} = \frac{3}{2 \times 30} 5 \times 10^{-3} = 2.5 \times 10^{-4} \text{ rad}. \qquad (14)$$

The height differences Δz can be found by integrating the gradient $\partial z/\partial x$ in the x-direction over the surface.

[3] These calculations were made by G. Bouwhuis of Philips Research Laboratories.

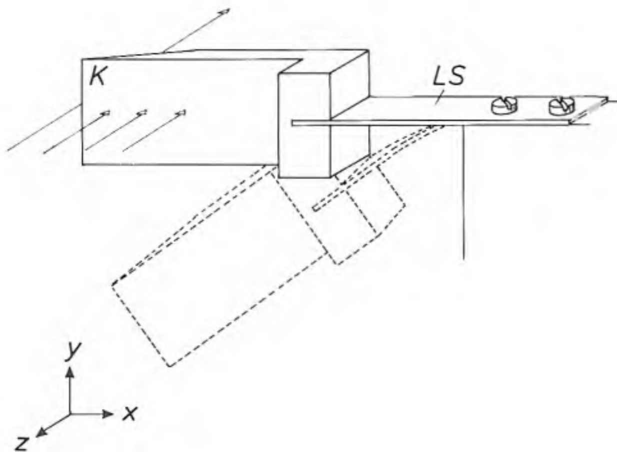

Fig. 6. The knife-edge K, which is connected to the system by a leaf spring LS, is correctly positioned by energizing a magnet. The movement takes place in the direction of the edge (y-direction), perpendicular to the optical axis (z-direction) and takes 50 ms. The edge of the knife is ground to prevent unwanted reflections in the direction of the diode array.

The inaccuracy of measurements over a distance of 1 µm (integration over one diode) is

$$\Delta z = \Delta \left(\frac{\partial z}{\partial x} \right) \Delta x.$$

In integration over a number of diodes the inaccuracy increases with the square of the number of measured points (statistically independent measurements), so that

$$\Delta z = \sqrt{n} \Delta \left(\frac{\partial z}{\partial x} \right) \Delta x.$$

Roughness measurements over a distance of 10 µm can be made to an accuracy of 0.75 nm. In profile measurements over a distance of 500 nm height differences can be determined to an accuracy of 5 nm.

The smallest distance in the object over which full contrast can be observed is $w = (f/h)\lambda = (30/3)0.8\mu m = 8\ \mu m$. Since the contrast decreases very slowly with w, the resolution is of the order of 5 µm.

A Schlieren microscope is illustrated schematically in *fig. 5*. The microscope has a conventional illumination system, consisting of a lamp, two lenses, an aperture diaphragm and a field diaphragm. The only difference from a conventional microscope is that the objective is replaced by an achromatic lens with a focal length of 30 mm and a numerical aperture of 0.2. This is necessary because it is not possible to place the knife-edge in the focal plane of a conventional microscope objective. The total magnification produced by the objective and the second lens of the imaging system is 13 times. The first beam-splitter, H_1, is used for illuminating the object, the second one, H_2, is required for viewing the image through an eyepiece and for focusing the microscope on the object. Since an experiment consists of four measurements, two with the knife-edge and two without it, it must be possible to reposition the knife-edge at exactly the same place after it has been removed from the microscope. The light intensity is measured to an accuracy of 0.1%, so that the reproducibility of the position of the knife-edge must also be 0.1%. This means that the position of the knife-edge must be adjustable within 1 µm of the optical axis, i.e. 0.1% of the dimension of the image of the source. The design of the knife-edge can be seen in *fig. 6*. It is attached to the optical system by two screws and a leaf spring. This meets the requirement that the knife-edge must

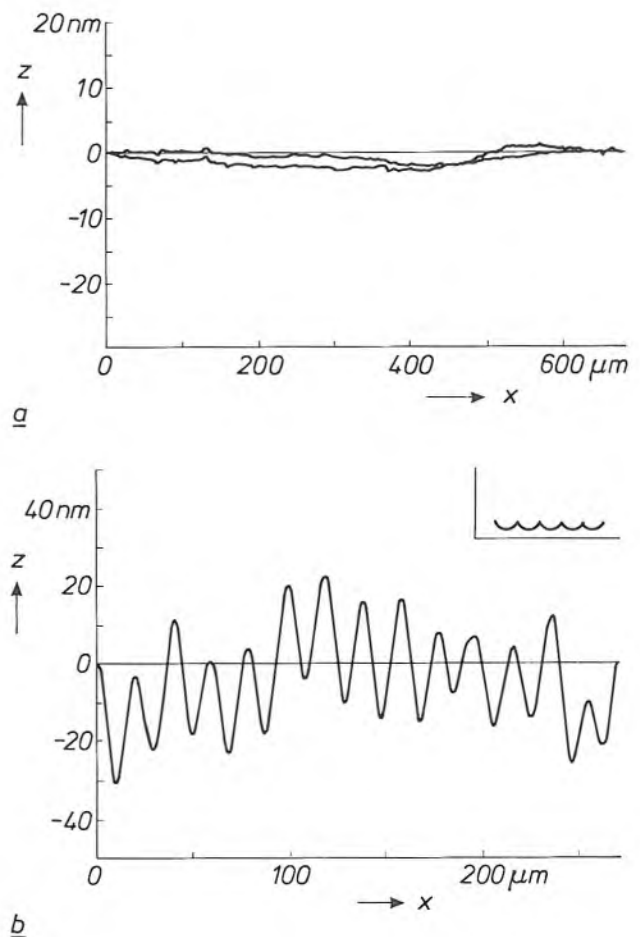

Fig. 7. a) A measurement of the height differences (z) of a highly polished surface as a function of position (x) on a line across the surface. The two curves represent two measurements made with the Schlieren microscope along the same line on the surface. In this case the surface asperities are of interest. The results of the measurements are digitally filtered with a highpass filter. This means that height variations of long wavelength (profiles) cannot be accurately reproduced. This appears from the fact that the two curves do not coincide, whereas small variations (roughness) in the two curves are indicated in the same way. b) A measurement of the height differences (z) on a surface that has been machined on a high-precision lathe by a diamond tool of radius 1 mm. This operation produces a pattern of grooves on the surface (*see inset*), with a pitch of 20 µm. The sharp edges found in such patterns are not visible because a lowpass filter cuts off the high spatial frequencies in these measurements.

always coincide with the optical axis to an accuracy of better than 1 μm.

The optical system alone as described above is not sufficient for making quantitative measurements. The light intensities are determined by a linear array of 1024 diodes, with a dynamic range better than 0.1%. The measured values are converted by an analog/digital converter into words of 10 bits and stored in the memory of a microcomputer. The microcomputer controls the measurements, checks the state of the components of the system and performs simple arithmetical operations (e.g. averaging). The actual calculations, the conversion of light intensities into gradients and height differences, and the numerical processing of the profile data, e.g. filtering or the determination of autocorrelation diagrams or Fourier spectra of the profile, is performed on a minicomputer. *Fig. 7* gives two examples of results obtained with the Schlieren microscope. Fig. 7*a* shows the roughness of a very smoothly polished surface, and fig. 7*b* the pattern of grooves produced on a surface by a tool in a high-precision lathe.

The employment of the Schlieren method in a microscope is only one of the possible applications. Similar methods (e.g. the Foucault method) can be used for quantitative measurements in the same way as described above. The method can also prove useful in cases where it is necessary to determine whether products meet certain criteria. In such a situation a perfect workpiece can be used as a reference surface. Any variations from the standard can then be immediately identified.

Summary. The Schlieren method, originally only used as a qualitative method for displaying the presence of gradients in the refractive index of transparent objects, is used for determining the shape and roughness of surfaces. A gradient in the refractive index is made visible by screening off a part of a light beam incident on an object. Accurate diodes for measuring the light intensity and the use of computers now make it possible to employ this method for quantitative determinations as well. The optical components do not have to satisfy any special conditions. Differential measurements are used, to correct for any imperfection in these components. The principle of the method has been successfully applied in a microscope. It is easy to use and insensitive to vibration, and therefore suitable for use in production conditions.

Television test decor

Picture quality with existing television technology is usually good. However, certain types of scene are notoriously difficult to capture and reproduce truly faithfully. Difficulties can arise if there are very large contrasts in brightness, strongly saturated colours, finely detailed patterns or highly reflecting surfaces. Research on new and better television systems does not only consist of theoretical studies, there are extensive experimental tests as well. To give the clearest possible comparison with existing systems, special studio decors are used. These contain as much 'difficult' scene material as possible, and the visual effect can be rather startling. The photograph shows some experimental test decor recently in use in the television studio at Philips Research Laboratories, Eindhoven. (In the next issue of this journal we shall give a detailed account of a new high-definition television system, HD-MAC, which gives greatly improved picture quality.)

Scientific publications

These publications are contributed by staff of laboratories and plants that form part of or cooperate with enterprises of the Philips group of companies, particularly by staff of the research laboratories mentioned below. The publications are listed alphabetically by journal title.

Laboratory	Code
Philips GmbH Forschungslaboratorium Aachen, Weißhausstraße, 5100 Aachen, Germany	*A*
Philips Research Laboratory, Brussels, 2 avenue Van Becelaere, 1170 Brussels, Belgium	*B*
Philips Natuurkundig Laboratorium, Postbus 80000, 5600 JA Eindhoven, The Netherlands	*E*
Philips GmbH Forschungslaboratorium Hamburg, Vogt-Kölln-Straße 30, 2000 Hamburg 54, Germany	*H*
Laboratoires d'Electronique et de Physique Appliquée, 3 avenue Descartes, 94450 Limeil-Brévannes, France	*L*
Philips Laboratories, N.A.P.C., 345 Scarborough Road, Briarcliff Manor, N.Y. 10510, U.S.A.	*N*
Philips Research Laboratories, Cross Oak Lane, Redhill, Surrey RH1 5HA, England	*R*

Authors	Lab	Title	Journal	Pages	Year
W. J. Bartels, J. Hornstra & D. J. W. Lobeek	*E*	X-ray diffraction of multilayers and superlattices	Acta Crystallogr. **A42**	539-545	1986
R. G. Gossink	*E*	Polymers for audio and video equipment	Angew. Makromol. Chem. **145/146**	365-389	1986
U. Enz	*E*	Bloch walls, solitons, particles: an analogy	Ann. Fond. Louis de Broglie **11** (no. 2)	87-100	1986
M. J. Verkerk & I. J. M. M. Raaymakers	*E*	Characterization of the topography of vacuum-deposited films. 1: Light scattering	Appl. Opt. **25**	3602-3609	1986
I. J. M. M. Raaymakers & M. J. Verkerk	*E*	Characterization of the topography of vacuum-deposited films. 2: Ellipsometry	Appl. Opt. **25**	3610-3615	1986
Luisa Gonzalez (*Univ. Madrid*), J. B. Clegg, D. Hilton, J. P. Gowers, C. T. Foxon & B. A. Joyce	*R*	Silicon migration during MBE growth of doped (Al, Ga)As films	Appl. Phys. A **41**	237-241	1986
J. Samitier*, J. R. Morante* (* *Univ. de Barcelona*), L. Giraudet & S. Gourrier	*L*	Optical behavior of the U band in relation to EL2 and EL6 levels in boron-implanted GaAs	Appl. Phys. Lett. **48**	1138-1140	1986
G. G. P. van Gorkom, A. van Oostrom, J. E. Crombeen & A. M. E. Hoeberechts	*E*	Cesium migration and equilibrium in a strong electric field on the surface of silicon	Appl. Phys. Lett. **49**	507-509	1986
A. H. van Ommen, B. H. Koek & M. P. A. Viegers	*E*	Amorphous and crystalline oxide precipitates in oxygen implanted silicon	Appl. Phys. Lett. **49**	628-630	1986
A. H. van Ommen, B. H. Koek & M. P. A. Viegers	*E*	Ordering of oxide precipitates in oxygen implanted silicon	Appl. Phys. Lett. **49**	1062-1064	1986
J. J. P. Bruines, R. P. M. van Hal, H. M. J. Boots, A. Polman* & F. W. Saris* (* *FOM, Amsterdam*)	*E*	Time-resolved reflectivity measurements during explosive crystallization of amorphous silicon	Appl. Phys. Lett. **49**	1160-1162	1986
C. Ronse	*B*	Definitions of convexity and convex hulls in digital images	Bull. Soc. Math. Belg. B **37**	71-85	1985
J. A. Pals	*E*	Basic properties in semiconductor devices	Crystalline semiconducting materials and devices, P.N. Butcher *et al.* (eds), Plenum, New York	507-548	1986
C. Niessen	*E*	Abstraction requirements in hierarchical design methods	Design Methodologies, S. Goto (ed.), Elsevier Science, Amsterdam	151-182	1986

H. J. Schouwenaars, E. C. Dijkmans, B. M. J. Kup* & E. J. M. van Tuijl* (**Philips Elcoma Div., Nijmegen*) *E*	A monolithic dual 16-bit D/A converter	IEEE J. **SC-21**	424-429	1986
M. Verhaegen & P. van Dooren *B*	Numerical aspects of different Kalman filter implementations	IEEE Trans. **AC-31**	907-917	1986
T. A. C. M. Claasen & W. F. G. Meclenbräucker *E*	Authors' reply to "Comments on 'Comparison of the convergence of two algorithms for adaptive FIR digital filters'"	IEEE Trans. **ASSP-34**	202-203	1986
A. J. E. M. Janssen, R. N. J. Veldhuis & L. B. Vries *E*	Adaptive interpolation of discrete-time signals that can be modeled as autoregressive processes	IEEE Trans. **ASSP-34**	317-330	1986
T. Krol *E*	(N,K) concept fault tolerance	IEEE Trans. **C-35**	339-349	1986
W. J. van Gils *E*	A triple modular redundancy technique providing multiple-bit error protection without using extra redundancy	IEEE Trans. **C-35**	623-631	1986
J. W. M. Bergmans *E*	Density improvements in digital magnetic recording by decision feedback equalization	IEEE Trans. **MAG-22**	157-162	1986
F. M. Dekking (*Univ. of Technol., Delft*) & P. J. van Otterloo *E*	Fourier coding and reconstruction of complicated contours	IEEE Trans. **SMC-16**	395-404	1986
A. Huizing *E*	Bereiding van zuiver kwartsglas door superkritisch drogen	Ing. Inf. Procestechnol. No. 10, 1986	19-23	1986
E. H. L. Aarts, F. M. J. de Bont, E. H. A. Habers & P. J. M. van Laarhoven *E*	Parallel implementations of the statistical cooling algorithm	Integration **4**	209-238	1986
J. G. Beerends* & A. J. M. Houtsma* (**Inst. Perception Res., Eindhoven*)	Pitch identification of simultaneous dichotic two-tone complexes	J. Acoust. Soc. Am. **80**	1048-1056	1986
J. 't Hart (*Inst. Perception Res., Eindhoven*)	Declination has not been defeated — A reply to Lieberman *et al.*	J. Acoust. Soc. Am. **80**	1838-1840	1986
J. A. Geurst *E*	Momentum-flux condition for Landau-Squire jet flow	J. Appl. Math. & Phys. **37**	666-672	1986
R. Schäfer (*Philips Lighting Div., Eindhoven*) & H.-P. Stormberg *A*	Particle number and pressure determination in high-pressure lamps	J. Appl. Phys. **60**	1263-1268	1986
F. J. A. den Broeder *E*	Layered magnetic domains in Fe-Cu multilayer films imaged by Schlieren-Lorentz microscopy	J. Appl. Phys. **60**	3381-3383	1986
M. H. L. M. van den Broek *E*	Electron-optical simulation of rotationally symmetric triode electron guns	J. Appl. Phys. **60**	3825-3835	1986
E. T. J. M. Smeets & A. M. W. Cox *E*	Influence of alkyl substituents of OMs and operating pressure on the quality of $In_x Ga_{1-x} As/InP$ heterostructures grown by OMVPE	J. Cryst. Growth **77**	347-353	1986
J. P. André, E. Dupont-Nivet, D. Moroni, J. N. Patillon, M. Erman & T. Ngo *L*	GaInP-AlGaInP-GaAs heterostructures grown by MOVPE at atmospheric pressure.	J. Cryst. Growth **77**	354-359	1986
B. J. Fitzpatrick, T. F. McGee III & P. M. Harnack *N*	Self-sealing and self-releasing technique (SSSR) for the crystal growth of II-VI compounds	J. Cryst. Growth **78**	242-248	1986
A. G. Tangena & G. A. M. Hurkx *E*	The determination of stress-strain curves of thin layers using indentation tests	J. Eng. Mater. & Technol. **108**	230-232	1986
R. B. Helmholdt (*ECN, Petten*), K. H. J. Buschow *E*	A neutron diffraction and magnetization study of PdMnTe	J. Less-Common Met. **123**	169-173	1986
J. J. van den Broek, J. L. C. Daams & R. Coehoorn *E*	Early proof of fivefold symmetry	J. Less-Common Met. **123**	L5-L7	1986
P. J. Severin, A. P. Severijns & C. H. van Bommel *E*	Passive components for multimode fiber-optic networks	J. Lightwave Technol. **LT-4**	490-495	1986
C. M. G. Jochem & J. W. C. van der Ligt *E*	Cooling and bubble-free coating of optical fibers at a high drawing rate	J. Lightwave Technol. **LT-4**	739-742	1986
G.-D. Khoe & A. H. Dieleman *E*	TTOSS: an integrated subscriber system for direct and coherent detection	J. Lightwave Technol. **LT-4**	778-784	1986

D. J. Broer & G. N. Mol	*E*	Fast curing primary buffer coatings for high strength optical fibers	J. Lightwave Technol. **LT-4**	938-941	1986
G.-D. Khoe, J. A. Luijendijk & L. J. C. Vroomen	*E*	Arc-welded monomode fiber splices made with the aid of local injection and detection of blue light	J. Lightwave Technol. **LT-4**	1219-1222	1986
P. Schobinger-Papamantellos (*Inst. für Kristallogr. und Petrogr., Zürich*) & K. H. J. Buschow	*E*	A neutron diffraction and magnetic study of the first-order phase transition in $TbGe_{1-x}Si_x$ ($0 < x < 0.4$)	J. Magn. & Magn. Mater. **62**	15-28	1986
M. J. Verkerk & W. A. M. C. Brankaert	*E*	Optical properties of reactively evaporated aluminium films	J. Mater. Sci. Lett. **6**	115-117	1987
J. W. M. Jacobs	*E*	Photochemical nucleation and growth of Pd on TiO_2 films studied with electron microscopy and quantitative analytical techniques	J. Phys. Chem. **90**	6507-6517	1986
A. A. van Gorkum & L. C. M. Beirens	*E*	Experiments on eliminating spherical aberration in electron guns using aspherical mesh lenses	J. Vac. Sci. & Technol. A **4**	2297-2306	1986
M. J. Verkerk & G. J. van der Kolk	*E*	Effects of oxygen on the growth of vapor-deposited aluminium films	J. Vac. Sci. & Technol. A **4**	3101-3105	1986
R. A. de Groot (*Univ. Nijmegen*), A. M. van der Kraan (*Interuniv. Reactor Inst., Delft*) & K. H. J. Buschow	*E*	FeMnSb: A half-metallic ferrimagnet	J. Magn. & Magn. Mater. **61**	330-336	1986
D. Washington	*R*	Colour display using the channel multiplier CRT	Jpn. Disp.	218-221	1986
W. J. A. Goossens	*E*	Tilt and temperature dependence of the pitch in the chiral smectic C phase	Liquid Cryst. **1**	521-528	1986
H. Baumgart, F. Phillipp (*Max Planck Inst., Stuttgart*) S. Ramesh, B. Khan, A. Martinez & E. Arnold	*N*	Twin stabilized planar growth of SOI films	Mater. Res. Soc. Symp. Proc. **53**	65-70	1986
B. A. Khan, T. Marshall, E. Arnold & R. Pandya	*N*	Leakage currents in p-channel accumulation mode TFT's	Mater. Res. Soc. Symp. Proc. **53**	435-439	1986
G. J. van der Kolk & M. J. Verkerk	*E*	Recrystallization of oxygen contaminated Al films	Mater. Res. Soc. Symp. Proc. **71**	357-362	1986
K. H. J. Buschow	*E*	New permanent magnet materials	Mater. Sci. Rep. **1**	1-63	1986
R. L. Bronnes & R. C. Sweet	*N*	The metallographic examination of an aluminium-titanium heat exchanger	Microstruct. Sci., Vol. 14, M.R. Louthan *et al.* (eds), Am. Soc. Met., Metals Park, OH	181-187	1986
L. J. van der Pauw	*E*	Light absorption in a bent dielectric slab with a lossy coating	Philips J. Res. **41**	431-444	1986
C. Colinet (*Lab. Thermodyn. & Physico-Chimie Metallurgique, St. Martin d'Hères*) & K. H. J. Buschow	*E*	Formation enthalpies of Gd-Pd and Gd-Pt compounds	Philips J. Res. **41**	445-451	1986
B. J. Fitzpatrick, P. M. Harnack & S. Cherin	*N*	Crystal growth of cadmium chalcogenides by the SSSR-zone melting method	Philips J. Res. **41**	452-459	1986
D. Snyers & A. Thayse	*B*	Theorem proving techniques and P-functions for logic design and logic programming	Philips J. Res. **41**	460-505	1986
P. J. Severin	*E*	Self-routing fibre-optic networks and switches using multi-tailed receiver/transmitter units	Philips J. Res. **41**	507-530	1986
J. Bergmans	*E*	Discrete-time models for digital magnetic recording	Philips J. Res. **41**	531-558	1986
T. N. Saadawi (*City Univ., New York*), N. Jain & M. Schwartz (*Columbia Univ., New York*)	*N*	Protocol for a distributed switching interactive CATV network	Philips J. Res. **41**	559-575	1986
R. S. Prodan	*N*	Multidimensional digital signal processing for television scan conversion	Philips J. Res. **41**	576-603	1986
C. B. Marshall	*R*	A radio-paging receiver architecture and demodulator	Philips J. Res. **41**, Suppl. no. 2	128 pp.	1986

D. C. Rogers*, J. Singleton*, R. J. Nicholas* (**Univ. Oxford*), C. T. Foxon & K. Woodbridge *R*	Magneto-optics in GaAs-$Ga_{1-x}Al_xAs$ quantum wells	Phys. Rev. B 34	4002-4009	1986
G. N. A. van Veen, F. H. M. Sanders, J. Dieleman, A. van Veen (*Interuniv. Reactor Inst., Delft*) D. J. Oostra* & A. E. de Vries* (**FOM, Amsterdam*) *E*	Anomalous time-of-flight distributions observed for argon implanted in silicon and resputtered by Ar^+-ion bombardment	Phys. Rev. lett. **57**	739-742	1986
F. J. C. M. Toolenaar & G. de With *E*	Translucent $Y_3Al_5O_{12}$. The influence of process parameters	Proc. Br. Ceram. Soc. **37**	241-246	1986
H. A. van Sprang & J. L. M. van de Venne *E*	Switching times for display application of the cholesteric to nematic phase transition	Proc. Eurodisplay Conf., Paris 1984	207-210	1984
H. Sari, L. Desperben & S. Moridi *L*	Optimum timing recovery for digital equalizers	Proc. GLOBECOM '85, New Orleans 1985	1460-1465	1985
A. F. de Jong, W. Coene* & D. van Dijck* (**Univ. Antwerpen*) *E*	*New methods for the construction of the phase-object function, to be used in dynamical electron diffraction calculations*	*Proc. Int. Cong. on Electron Microscopy, Kyoto 1986*	*503-504*	*1986*
B. H. Verbeek *E*	Coherence properties and l.f. noise in AlGaAs lasers with optical feedback	Proc. SPIE **587**	93-98	1986
A. A. Turnbull *R*	The application of heat-collector fins to reticulated pyroelectric arrays	Proc. SPIE **588**	38-43	1986
C. H. L. Weijtens & W. C. Keur *E*	Reduction of reflection losses in solid-state image sensors	Proc. SPIE **591**	75-79	1986
J. O. Voorman *E*	Analog integrated filters or continuous-time filters for LSI and VLSI	Rev. Phys. Appl. **22**	3-14	1987
A. J. Kil*, R. J. J. Zijlstra*, P. M. Koenraad* (**Univ. Utrecht*), J. A. Pals, J. P. André *E,L*	Noise due to localized states in the quantum Hall regime	Solid State Commun. **60**	831-834	1986
R. Houdré*, C. Hermann*, G. Lampel* (**Ecole Polytech. Palaiseau*) & P. M. Frijlink *L*	Photoemission study of a single GaAlAs/GaAs/GaAlAs quantum well	Surf. Sci. **168**	538-545	1986
E. E. Havinga & L. W. van Horssen *E*	Dependence of the electrical conductivity of heavily-doped poly-p-phenylenes on the chain length	Synth. Met. **16**	55-70	1986
F. Baaijens *E*	On a numerical method to solve contact problems	Thesis, Eindhoven	121 pp.	1987
M. van den Broek *E*	The design of rotationally symmetric triode electron guns	Thesis, Eindhoven	127 pp.	1986
B. Greenberg, W. K. Zwicker & I. Cadoff *N*	ZnS epitaxy on sapphire (110)	Thin Solid Films **141**	89-97	1986
P. C. Zalm *E*	Ion-beam assisted etching of semiconductors	Vacuum **36**	787-797	1986
J. H. Waszink & M. J. Piena *E*	Experimental investigation of drop detachment and drop velocity in GMAW	Weld. J. **65** (Weld. Res. Suppl.)	289s-298s	1986
R. E. van de Leest *E*	On the atmospheric corrosion of thin copper films	Werkstoffe & Korrosion **37**	629-632	1986

Contents of Philips Telecommunication and Data Systems Review **44**, No. 3, 1986

R. F. Wielinga & J. Preston: The new medium of Compact Discs, and introduction to Optical Disc Recording (pp. 2-6)

M. G. Noordenbos: CD-ROM; User aspects and application fields (pp. 7-17)

K. Meissner: Device, system integration and standardization (pp. 18-31)

J. P. H. Maat: Call processing in a fully integrated network of SOPHO-S2500 PABX's (pp. 32-45)

Volume 43, No. 7 pages 169-196 Published 13th July 1987

H. J. Ligthart and J. Politiek: An open 800-kV ion-implantation machine,

Philips Tech. Rev. **43**, No. 7, 169-179, July 1987.

Since the high-voltage section of the ion-implantation machine developed at Philips Research Laboratories is not insulated by gas under pressure in a tank, changing the ion source is relatively easy. The machine is therefore particularly suitable for research. The accelerating voltage is high, 800 kV, so that heavy elements can be implanted in heavy substrates. There are two target chambers, one designed for treating silicon slices for IC manufacture, the other designed for other samples, including metals. The half-width of the beam cross-section and the location of the pattern of the beam scan on the sample are evaluated with the aid of a wire frame around the sample; the wire frame is earthed through a milliammeter. The implantation dose is measured with a Faraday cup. Several ion sources have been tested. Some examples are given to demonstrate the usefulness of the machine: implantation of buried oxygen layers in a silicon slice, implantation of aluminium to improve the corrosion resistance of copper, and the determination of a number of concentration profiles for phosphorus in silicon at different energies.

R. J. Asjes, C. S. Caspers and C. H. F. Velzel: A laser-Doppler displacement meter,

Philips Tech. Rev. **43**, No. 7, 180-182, July 1987.

In the manufacture of products such as wire and cable it is often necessary to measure the length of the quantity produced. The Philips Centre for Manufacturing Technology (CFT) has developed a displacement meter that operates on the laser-Doppler principle. A laser beam is split by a rotating grating into two beams that are made to intersect. In the volume where the intersection occurs an interference pattern of moving planes is produced. An image of this interference pattern is produced on the material whose length is to be measured. A particle that moves through the interference volume will scatter light at a frequency that depends on its own velocity and on the velocity of the planes of the interference pattern. This frequency is measured and is also kept more or less constant by controlling the rate of rotation of the grating as a function of the velocity of the passing material. The velocity and the displacement of the passing material can be calculated from the frequency actually measured and from the frequency due to the rotation of the grating the velocity and the displacement of the passing material can be calculated. The instrument is controlled by a microcomputer and gives a reading of the velocity and the length of the material every second. The inaccuracy of the measurement is less than 0.2%.

PHILIPS

G. Prast: Quantitative measurements by the Schlieren method,
Philips Tech. Rev. **43**, No. 7, 184-191, July 1987.

The Schlieren method, originally only used as a qualitative method for displaying the presence of gradients in the refractive index of transparent objects, is used for determining the shape and roughness of surfaces. A gradient in the refractive index is made visible by screening off a part of a light beam incident on an object. Accurate diodes for measuring the light intensity and the use of computers now make it possible to employ this method for quantitative determinations as well. The optical components do not have to satisfy any special conditions. Differential measurements are used, to correct for any imperfection in these components. The principle of the method has been successfully applied in a microscope. It is easy to use and insensitive to vibration, and therefore suitable for use in production conditions.

I wish to subscribe to

PHILIPS TECHNICAL REVIEW

(date) (signature)

Please tick the appropriate box

Regular subscription 80 guilders or U.S. $ 35.00 per volume ☐

The subscription includes postage and will start with Vol. 43, No. 1.
Please pay when you receive our invoice.

Student's subscription 32 guilders or U.S. $ 14.00 per volume ☐

Please send a copy of your student's card or other written proof that you are a student; valid for two volumes.

Name

Initials

Title

Address

stamp

as

postcard

Administration Department
Philips Technical Review

Philips Research Laboratories
Building WY 136

P.O. Box 80 000

5600 JA Eindhoven
The Netherlands

OTHER PHILIPS PUBLICATIONS

Philips Journal of Research

A publication in English on the research work carried out in the various Philips laboratories. Published in annual volumes of six issues each of about 100 pages, size 15½ × 23½ cm.

Philips Telecommunication and Data Systems Review

A publication in English, dedicated to systems and equipment for business communications, computer systems and networks, telecommunication services, radio communications and dictation. Published in volumes of four issues, about 40 pages per issue, size 21½ × 29½ cm.

Electronic Components and Applications

A publication in English, containing articles dealing with the theory and practice of electronic components and materials. Four issues per year, about 60 pages per issue, size 21 × 29½ cm.

Medicamundi

A publication in English on radiology, nuclear medicine and medical electronics. Three issues per volume, about 60 pages per issue, size 21 × 29½ cm.

Forthcoming issues of Philips Technical Review will include articles on:

Automatic speech segmentation

A mobile system for image bulk storage

Industrial glass production

Philips Tech. Rev. Vol. 43, No. 7, July 1987

Contents

Page

An open 800 kV ion-implantation machine . . . . H. J. Ligthart and J. Politiek 169

A laser-Doppler displacement meter . . . . R. J. Asjes, C. S. Caspers and C. H. F. Velzel 180

Then and now (1937-1987) 183

Quantitative measurements by the Schlieren method . . . . G. Prast 184

Television test decor 192

Scientific publications 193

PHILIPS TECHNICAL REVIEW
Philips Research Laboratories
P.O. Box 80 000
5600 JA Eindhoven
The Netherlands

Subscription rate per volume	fl. 80.00 or U.S. $ 35.00
Student's subscription	fl. 32.00 or U.S. $ 14.00
Binder	fl. 10.00 or U.S. $ 4.00

Payment only after invoicing, please.

Printed in the Netherlands

PHILIPS